CRYSTAL GROWTH & DESIGN

Article

Crystal engineering applied to modulate the structure and magnetic properties of oxamate complexes containing the [Cu(bpca)] cation

Willian X. C. Oliveira, Carlos B. Pinheiro, Marinez M. da Costa, Ana P. S. Fontes, Wallace C. Nunes, Francesc Lloret, Miguel Julve, and Cynthia L.M. Pereira

Cryst. Growth Des., **Just Accepted Manuscript** • DOI: 10.1021/acs.cgd.6b00613 • Publication Date (Web): 13 Jun 2016

Crystal engineering applied to modulate the structure and magnetic properties of oxamate complexes containing the $[Cu(bpca)]^+$ cation

Willian X. C. Oliveira,[†] Carlos B. Pinheiro,[‡] Marinez M. da Costa,[§] Ana P. S. Fontes,[⊥] Wallace C. Nunes,[‖] Francesc Lloret,[⊗] Miguel Julve[⊗] and Cynthia L. M. Pereira[†]*

[†]Departamento de Química, Instituto de Ciências Exatas, Universidade Federal de Minas Gerais. Av. Pres. Antônio Carlos, 6620, Pampulha, 31270-901, Belo Horizonte, Minas Gerais, Brasil;

[‡]Departamento de Física, Instituto de Ciências Exatas, Universidade Federal de Minas Gerais. Av. Pres. Antônio Carlos, 6620, Pampulha, 31270-901, Belo Horizonte, Minas Gerais, Brasil;

[§]Instituto Federal de Educação, Ciência e Tecnologia do Sudeste de Minas Gerais, IFSEMG, 36080-001, Juiz de Fora, Brazil.

[⊥]Departamento de Química, Instituto de Ciências Exatas, Universidade Federal de Juiz de Fora, 36036-900, Juiz de Fora, MG, Brazil.

[‖]Instituto de Física, Universidade Federal Fluminense, 24210-346, Niterói, RJ, Brazil;

[⊗]Instituto de Ciencia Molecular/Departament de Química Inorgànica, Universitat de València, C/ Catedrático José Beltrán 2, 46980 Paterna, València, Spain.

ABSTRACT

This work deals with the crystal engineering features of four related copper(II)-based compounds with formulas $\{[\{Cu(bpca)\}_2(H_2ppba)]\cdot 1.33dmf\cdot 0.66dmso\}_n$ (**2**), $[\{Cu(bpca)(H_2O)\}_2(H_2ppba)]$ (**3**), $[\{Cu(bpca)\}_2(H_2ppba)]\cdot dmso$ (**4**), and $[\{Cu(bpca)\}_2(H_2ppba)]\cdot 6H_2O$ (**5**) [H_4ppba = *N*,*N*'-1,4-phenylenebis(oxamic acid) and Hbpca = bis(2-pyridylcarbonyl)amide] and how their distinct molecular and crystal structures translate into their different magnetic properties. **2** and **3** were obtained

through the hydrolytic reaction of the double-stranded oxamato-based dipalladium(II) paracyclophane precursor of formula $[\{K_4(H_2O)_2\}\{Pd_2(ppba)_2\}]$ (**1**) with the mononuclear copper(II) complex, $[Cu(bpca)(H_2O)_2]^+$, either in a water-dmso-dmf solvent mixture or in water, respectively. The straightforward reaction of the neutral H_4ppba molecule with $[Cu(bpca)(H_2O)_2]^+$ in a water-dmso mixture afforded compound **4** whereas compound **5** resulted from the reaction between the copper(II) complex and the K_2ppba salt in water. The $[Pd_2(ppba)_2]^{4-}$ tetraanionic unit, which is present in **1** has a [3,3] metallacyclophane-type motif connected by two N–Pd–N bonds. This entity acts as a ligand towards partially hydrated potassium(I) cations through its outer oxamate oxygens leading to a neutral 3D network. The structure of **2** consists of neutral chains made up by double oxo(carboxylate-oxamate)-bridged di[{bis(2-pyridylcarbonyl)amidate}copper(II)] units are which connected by the extended H_2ppba^{2-} ligand, each of its oxamate fragment adopting a bidentate/outer monodentate coordination mode. Compounds **2**-**5** are neutral and centrosymmetric dicopper(II) complexes which have in common the presence of peripheral bpca ligands and H_2ppba^{2-} as a bridge with each of its monoprotonated oxamate groups exhibiting a rare monodentate (**3**) and bis-bidentate (**4** and **5**) coordination modes. Compounds **2**, **4** and **5** share the same basic $[\{Cu(bpca)\}_2(H_2ppba)]$ unit, but besides the difference in cocrystallization solvent molecules and synthetic strategies they features very different crystal structures. To better understand the role of palladium(II) ions in the formation of **2** and **3**, some studies were carried on using different mixtures of solvents such as water, dmso and dmf which revealed a major importance of dmf in the formation of **2** and the dependence on the palladium(II) ions in the formation of **3**. A reaction pathway leading to the formation of **2** and **3** is then proposed. The variable-temperature (2.0–300 K) magnetic susceptibility measurements of **2**, **4**, and **5** revealed the occurrence of weak

ferro- [J = +0.70 cm^{-1} (**2**)] and antiferromagnetic interactions [J = –0.90 (**4**) and –0.79 cm^{-1} (**5**)], the spin Hamiltonian being defined as $\mathbf{H} = -J\,\mathbf{S}_1 \cdot \mathbf{S}_2$. The different nature and strength of the magnetic coupling along this unique series of compounds are discussed in the light of the structural data and they are compared with those of related dicopper(II) systems.

INTRODUCTION

In the last years, many research teams worldwide have focused on the crystal engineering and supramolecular chemistry envisaging to make crystals by design, trying to control the molecular ordering of organic or metal-organic building blocks in the solid state to obtain desirable materials with interesting properties.[1-4] However, the control of the self-organization in the solid state is a hard task since many factors are involved such as the temperature, concentration of the reactants and type of solvents, for instance.[5] Dealing with the role of solvents on the synthesis of metal-organic compounds, they are able to modulate the physical properties of the materials for their applications in several areas such as gas storage and separation, catalysis, magnetism and optics.[6] Solvents can be polar and nonpolar, and the polar ones can be aprotic or protic and thus may favor the hydrogen bonding. These different characteristics of the solvents have to taken into account during the synthesis of metal-organic compounds, because they can result in the formation of very similar compounds with different structural and physical properties.

Several years ago, Kahn and co-workers developed the concept of "molecular magnetic sponge" in their pioneering work in the field of molecular magnetism.[7] They show how the compound of formula [CoCu(obbz)(H_2O)$_4$](H_2O)$_2$ [H_4obbz = *N*,*N'*-bis(2-

carboxyphenyl)oxamide] changes drastically its magnetic properties passing from a nonmagnetic state to a ferromagnetic one with a Curie temperature (T_C) of 30 K by structural conversion from a chain (1D) to a bidimensional (2D) network of formula $[CoCu(obbz)(H_2O)]_n$ after hydration/dehydration. More recently, transmetallation was reported for the paramagnetic three-dimensional (3D) metal-organic framework (MOF) of formula $Mg^{II}_2\{Mg^{II}_4[Cu^{II}_2(Me_3mpba)_2]_3\}\cdot 45H_2O$ [Me_3mpba =*N*,*N*'-2,4,6-trimethyl-1,3-phenylenebis(oxamate)] resulting in two novel porous magnets of formulas $Co_2^{II}\{Co^{II}_4[Cu^{II}_2(Me_3mpba)_2]_3\}\cdot 56H_2O$ and $Ni_2^{II}\{Ni^{II}_4[Cu^{II}_2(Me_3mpba)_2]_3\}\cdot 54H_2O$ by immersing single crystals of the parent Mg^{II} compound into saturated aqueous solutions of $M^{II}(NO_3)_2\cdot 6H_2O$ (M = Co and Ni, respectively) for several weeks.[8]

Focusing on oxamate-based systems, some examples recently reported feature the conversion of the starting building blocks during the crystallization process.[9-12] For instance, the reaction of the dicopper(II) complex, $[Cu_2(edpba)_2]^{4-}$, [H_4edpba = *N,N'*-2,2′-ethylenediphenylenebis(oxamic acid)] with manganese(II) ions afforded the wheel-like complex of formula $[Mn_5Cu_5(edpba)_5(dmso)_7(H_2O)_5]$ where a novel pentanuclear $[Cu_5(edpba)_5]^{10-}$ entity occurs.[9] In addition, the mononuclear nickel(II) complex, $[Ni(H_2edpba)(bipy)]$ (bipy = 2,2'-bipyridine) in presence of fully solvated free copper(II) ions results in the heterobimetallic $[CuNi(H_2edpba)(bipy)]_n$ polymer that undergoes further transmetallation and transforms into the chain-like compound $[Cu(H_2edpba)(bipy)]_n$.[10] Finally, the partial hydrolysis of the oxamate fragments of the $opba^{4-}$ ligand turning into oxalate in the reaction of the $[Cu(opba)]^{2-}$ complex [H_4opba = *N,N'*-1,2-phenylenebis(oxamic acid)] with manganese(II) ions in dmso accounts for the formation of the 2D compound $(Bu_4N)_{2n}[Mn_2\{Cu(opba)\}_2(ox)]_n$ (Bu_4N^+ = tetra-*n*-butylammonium cation and ox = oxalate).[11] Initially this compound was previously obtained in very low yield, relying on the slow hydrolysis of $[Cu(opba)]^{2-}$ building

block. After understanding the whole process, a simpler and faster synthetic pathway was proposed using simpler reactants which lead to the desired product with a higher purity grade.

In our own current research work with oxamate-based complexes, a temperature dependence also was observed on the reactions and crystallization processes involving the $[Pd(opba)]^{2-}$ and $[Cu(bpca)(H_2O)_2]^{+}$ building blocks [Hbpca = bis(2-pyridylcarbonyl)amide].[12] The trinuclear compound of formula $\{[Cu(bpca)]_2[Pd(opba)]\}\cdot 1.75dmso\cdot 0.25H_2O$ is obtained when the solution is cooled fast whereas the 1D zigzag polymer $\{[Cu(bpca)]_2[Pd(opba]\}_n\cdot n$dmso results when slowing down the cooling process is slow. Temperature also affects the reaction between manganese(II) ions and dicopper(II) compound $[Cu_2(mpba)_2]^{4-}$ [H_4mpba = *N,N'*-1,3-phenylenebis(oxamic acid)].[13] Crystallization tests carried out at 16 ºC afforded the stair-like chain $\{[trans\text{-}Mn(H_2O)_2]_2[Cu_2(mpba)_2]\}_n$, whereas the linkage of the chains leading to a 2D network of formula $\{[trans\text{-}Mn(H_2O)_2]_2[Cu_2(mpba)_2(H_2O)_2]\}_n$[14] is obtained at room temperature.

The pH control is also of fundamental relevance in terms of protonation/deprotonation of the amide group from the oxamate ligands.[15] For instance, fully protonated H_4edpba species shows interconversion between the neutral dicopper(II) complex $[Cu_2(H_2edpba)_2(EtOH)_2]$ synthesized in acidic medium [a pale green solid exhibiting ferromagnetic coupling between the copper(II) ions] and the dicopper(II) salt $(Bu_4N)_2[Cu_2(edpba)_2]$ obtained under basic conditions (a dark green paramagnetic complex).[16] The pH variation in this example, could be also used as a trigger for the switch of two different structures resulting in distinct magnetic properties.[16] In another example, the partial hydrolysis of the diethyl ester derivative

Et_2H_4opba in the presence of the $[Cu(bpca)(H_2O)_2]^+$ complex under acidic conditions (pH *ca.* 3.8) yielded the 1D coordination polymer $[Cu(bpca)(EtH_2opba)]_n$.[17]

In an earlier work, we proved that the solvent plays an important role in the interconversion of the dinuclear complex $[Cu(H_2mpba)(bipy)]_2 \cdot 2H_2O$ into the chain compound $[Cu(H_2mpba)(bipy)]_n \cdot dmso$.[18] Both compounds can be isolated by the reaction between $[Cu(bipy)Cl_2]$ and K_2H_2mpba in water and water-dmso mixtures, respectively. Even more surprisingly, when dmso is added to the dicopper(II) complex, it is transformed into the chain which in turn goes back to the discrete structure after heating in water, establishing a cyclic conversion process.

It is important to emphasize that the structural differences observed in these compounds led to distinct magnetic properties.[19-23] Thus, the investigation of the crystallization process is very important in order to get a better understanding of the chemistry that rules beyond the oxamate-based systems and all the efforts devoted to achieve more efficient methods to control the resulting molecular architectures by means of crystal engineering will be required on the long way from the design to the wanted crystal.

In the present work, we investigate the role played by the solvent and the palladium(II) ion on the formation of two new copper(II) complexes from the palladium-oxamate based $[Pd_2(ppba)_2]^{4-}$ anion and the $[Cu(bpca)]^+$ cation [H_4ppba = *N,N'*-1,4-phenylenebis(oxamic acid)] (see Scheme 1).

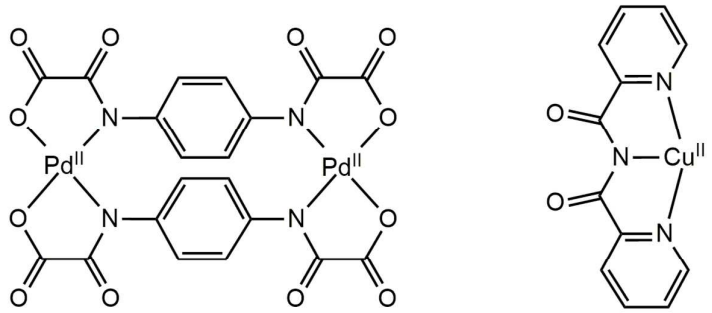

[Pd$_2$(ppba)$_2$]$^{4-}$ **[Cu(bpca)]$^{+}$**

Scheme 1. Structural formula of the palladium-oxamate based [Pd$_2$(ppba)$_2$]$^{4-}$ anion and the [Cu(bpca)]$^{+}$ cation.

Hence, the chain {[{Cu(bpca)}$_2$(H$_2$ppba)]·1.33dmf·0,66dmso}$_n$ (**2**) and the dinuclear complex [{Cu(H$_2$O)(bpca)}$_2$(H$_2$ppba)] (**3**) were obtained by reacting solutions of K$_4$[Pd$_2$(ppba)$_2$]·2H$_2$O (**1**) and [Cu(bpca)(H$_2$O)$_2$]NO$_3$·2H$_2$O in a water-dmso-dmf solvent mixture and water, respectively (Scheme 2). Reactions using [Cu(bpca)(H$_2$O)$_2$]NO$_3$·2H$_2$O and the K$_2$H$_2$ppba salt or the H$_4$ppba acid were carried out in different solvent combinations involving water, dmso and dmf in order to investigate the synthetic pathway leading to **2** and **3**. These attempts afforded instead the new dinuclear complexes [{Cu(bpca)}$_2$(H$_2$ppba)]·2dmso (**4**) and [{Cu(bpca)}$_2$(H$_2$ppba)]·6H$_2$O (**5**) (Scheme 2). It deserves to be noted that the coordination polymer **2** and the discrete dinuclear complexes **4** and **5** show the same basic [{Cu(bpca)}$_2$(H$_2$ppba)] unit, which is similar to [{Cu(bpca)(H$_2$O)}$_2$(H$_2$ppba)] entity observed in **3**. They differ in the synthetic strategy and in the packing of the solvent contents. In the context of the present work, this is a key point since the crystal engineering led to products of different dimensionality and different magnetic behaviors, as will be discussed in the next sections. The preparation and structural characterization of **1** is described herein together with the magnetic properties of **2**, **4**

and **5** following a comparative study of the relationship between the synthetic pathway, crystal structures and magnetic properties.

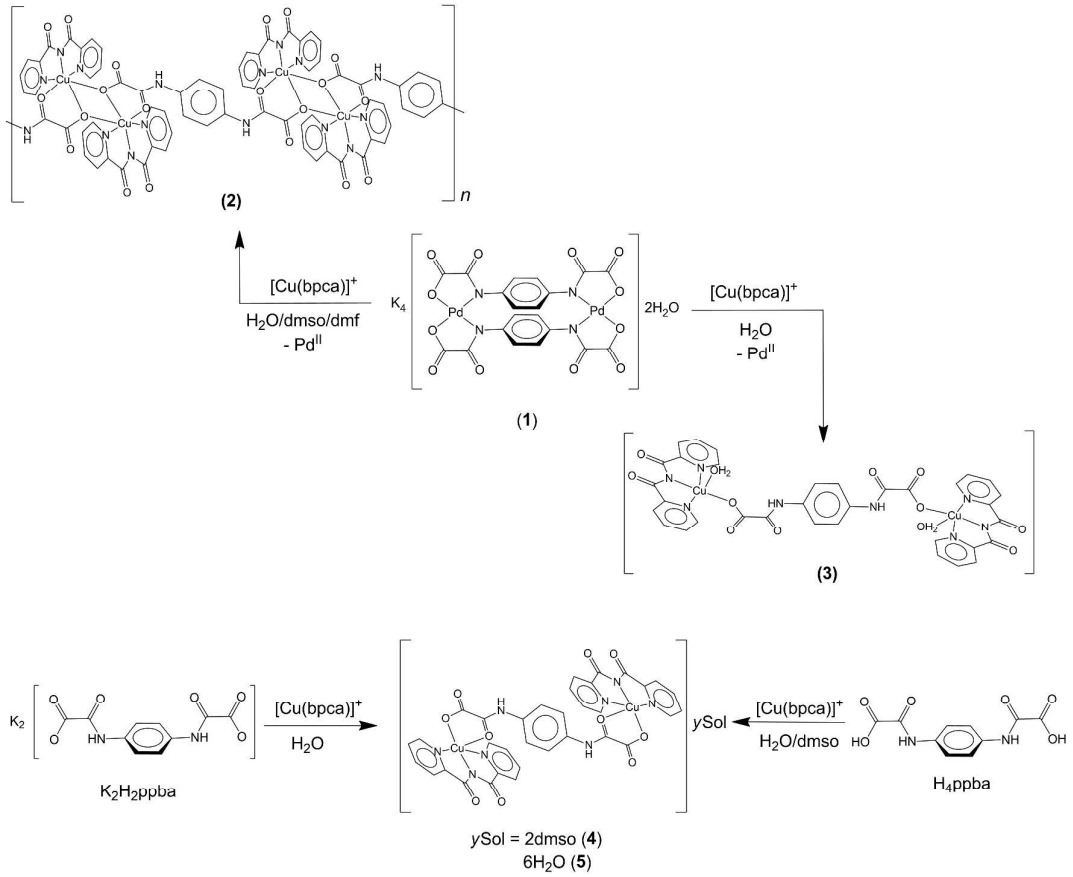

Scheme 2. Different synthetic routes leading to the complexes **2**–**5**.

EXPERIMENTAL SECTION

General Information. All of the chemicals for the syntheses were obtained from commercial sources (Sigma Aldrich and Merck) and used without further purification. The diethyl ester derivative Et_2H_2ppba and the mononuclear complex $[Cu(bpca)(H_2O)_2]NO_3 \cdot 2H_2O$ were synthetized as reported previously.[24,25] Elemental analysis (C, H and N) were carried out on a Perkin-Elmer 2400 analyser. The copper

contents was determined by atomic absorption spectrometry with a Hitachi Z-8200 polarized atomic absorption spectrophotometer.

Synthesis of K_2H_2ppba. Solid Et_2H_2ppba (0.308 g, 1.00 mmol) was added to an aqueous solution (30 mL) containing KOH (0.165 g, 2.50 mmol). The suspension was kept under stirring at 50 ^oC for 1 h. The addition of 20 mL of acetone to the resulting solution caused the precipitation of a white solid, which was filtered off and washed with acetone and diethyl ether. The solid was dried at room temperature for 24 h. Yield: 85% (0.279 g, 0.85 mmol). Anal. Calcd. for $C_{10}H_6N_2O_6K_2$ (328.3 g mol^{-1}): C, 36.45; H, 1.31; N, 8.72. Found: C, 36.58; H, 1.36; N, 8.63 %. IR (KBr disk/cm^{-1}): 3333 [ν(O–H)], 3354 [ν(N–H)], 1675 [ν(C=O)], 1640 [ν(C=O)], 1540 [ν(C=C)], 1540 [ν(CO_2^-)], 830 and 729 [ν(C–H)].

Synthesis of H_4ppba. Solid Et_2H_2ppba (0.308 g, 1.00 mmol) was added to an aqueous solution (30 mL) containing KOH (0.165 g, 2.50 mmol). The suspension was kept under stirring at 50 ^oC for 1 h. The resulting solution was cooled down to room temperature and 4.0 mol L^{-1} HCl was added dropwise until pH = 2.0. The white solid that separated was collected by filtration, washed with ethanol and diethyl ether and dried at low pressure for 24 h. Yield: 91% (229 mg, 0.91 mmol). Anal. Calcd. for $C_{10}H_8N_2O_6$ (252.6 g mol^{-1}): C, 47.01; H, 2.94; N, 10.87. Found: C, 47.10; H, 3.05; N, 11.01%. IR (KBr disk/cm^{-1}): 3333 [ν(O–H)], 3306 [ν(N–H)], 1734 [ν(C=O)], 1656 [ν(C=O)], 1571 [ν(C=C)], 851 and 726 [δ(C–H)]. ^1H NMR (200 MHz, dmso-d_6/$CDCl_3$ 4:1, ppm): 7.72 (s, 4H, C_{ar}–H) and 10.61 (s, 2H, N_{amide}–H). ^{13}C NMR (75 MHz, dmso-d_6/$CDCl_3$ 4:1, ppm): 128.88, 134.41, 156.73 and 162.27.

*Synthesis of $[\{K_4(H_2O)_2\}\{Pd_2(ppba)_2\}]$ (**1**).* Solid Et_2H_2ppba (0.308 g, 1.00 mmol) was added to an aqueous solution (10 mL) containing Et_4NOH (1.44 mL, 4.00 mmol, 20% weight in water) under stirring at 50 ^oC for 1 h. Then the solution was

cooled down to room temperature and an aqueous solution (4.00 mL) containing $K_2[PdCl_4]$ (0.328 g, 1.00 mmol) was slowly added, under vigorous stirring. The dark red solution was kept under stirring for 24 h. After this time, the resulting mixture of products were centrifuged several times at 5000 rpm. The yellow powder was collected and then filtered off, washed with ethanol and diethyl ether and dried at room temperature for 24 h. Yield: 75% (0.717 g, 0.75 mmol). Rhombic shape single crystals of **1** were grown by recrystallization of the yellow solid in aqueous solution. Anal. Calcd. for $C_{20}H_{16}N_4O_{16}K_4Pd_2$ (910.6 g mol^{-1}, **1**): C, 25.58; H, 1.82; N 5.76. Found: C, 25.70; H, 1.91; N, 5.84%. IR (KBr disk/cm^{-1}): 3419 [ν(O–H)], 1634 [ν(C=O)], 1604 [ν(C=C)], 1380 [ν(CO_2^-)], 831 [δ(C–H)] and 523 [ν(Pd–O)]. ^{1}H NMR (200 MHz, D_2O, ppm): 6.34 (s, 4H).

*Synthesis of {[{Cu(bpca)}$_2$(H$_2$ppba)]·1.33dmf·0.66dmso}$_n$ (**2**).* A dmso solution (1.0 mL) of **1** (25 mg, 27.6 mmol) was carefully deposited at the bottom of a long glass test tube (20 mL capacity, 15 cm height). Then, a H_2O-dmso-dmf mixture (1:1:1 v/v/v, 15 mL) was added dropwise and finally, an aqueous solution (5.0 mL) of $[Cu(bpca)(H_2O)_2]NO_3{\cdot}2H_2O$ (16.0 mg, 32.3 mmol) was placed on the top. The tube was covered by parafilm® and the diffusion of the reactants was allowed for 30 days under ambient temperature. X-ray quality deep blue plates of **2** that grew during this time were collected by filtration, washed with the H_2O-dmso-dmf solvent mixture (1:1:1 v/v/v) and dried under the open air for 48 h. Yield: 20% (6.6 mg, 3.1 μmol). This compound can also be synthetized by using H_4ppba (25 mg, 99.2 μmol) instead of **1** through the previous procedure, in the same solvent mixture. Yield: 73% (24.8 mg, 0.011 mmol). Anal. Calcd. for $C_{39.33}H_{35.33}N_{9.44}O_{12}S_{0.66}Cu_2$ (979.2 g mol^{-1}, **2**): C, 48.08; H, 3.52; N, 13.30; Cu, 13.05. Found: C, 48.14; H, 3.61; N, 13.35; Cu, 12.98%. IR (KBr disk/cm^{-1}): 3271 [ν(N–H)], 1717 [ν(C=O)], 1676 [ν(C=O)], 1651 [ν(C=O)], 1599 [ν(C=C)], 1540

[ν(CO_2^-)], 1285 [ν(C–N)], 1025 [ν(S=O)], 827 and 705 [δ(C–H)], 768 [δ(C–H)] and 487 [ν(Cu–O)].

*Synthesis of [{Cu(H_2O)(bpca)}$_2$(H_2ppba)] (**3**).* Solid samples of **1** (10.0 mg, 10.0 μmol) and [Cu(bpca)(H_2O)$_2$]NO_3·2H_2O (10.0 mg, 20.1 μmol) were placed respectively at the bottom of the arms of a 5.0 mL capacity H-shaped tube. The tube was filled with water covered with parafilm®, and the reactants were allowed to diffuse at room temperature. A few plate-like deep blue single crystals of **3** were grown after three months, but they are not representative of the green powder which was formed together. The stoichiometry of **3** was determined by X-ray diffraction on single crystals, further studies on **3** being precluded because of the very low yield.

*Synthesis of [{Cu(bpca)}$_2$(H_2ppba)]·dmso (**4**).* A dmso solution (1.0 mL) of H_4ppba (20.0 mg, 79.4 μmol) was placed at the bottom of a long test tube. A water:dmso mixture (1:1 v/v, 18.0 mL) was carefully added and followed by the dropwise addition of an aqueous solution (2.0 mL) containing [Cu(bpca)(H_2O)$_2$]NO_3·2H_2O (16.0 mg, 30.1 μmol). The reactants were allowed to diffuse at room temperature. X-ray quality blue plates of **4** were obtained after 30 days. They were collected by filtration, washed with a small amount of a water:dmso mixture (1:1 v/v) and left to dry at room temperature for 48 h. Yield: 65% (9.3 mg, 0.01 mmol). Anal. Calcd. for $C_{36}H_{28}N_8O_{11}SCu_2$ (829.7 g mol^{-1}, **4**): C, 45.57; H, 3.42; N, 11.95; Cu, 14.25. Found: C, 45.63; H, 3.50; N, 12.05; Cu, 14.10%. IR (KBr disk/cm^{-1}): 3337 [ν(N–H)], 1717 [ν(C=O)], 1676 [ν(C=O)], 1645 [ν(C=O)], 1604 [ν(C=C)], 1540 [ν(CO_2^-)], 1290 [ν(C–N)], 1025 [ν(S=O)], 827 and 705 [δ(C–H)], 768 [δ(C–H)] and 494 [ν(Cu–O)].

*Synthesis of [{Cu(bpca)}$_2$(H_2ppba)]·6H_2O (**5**).* Solid samples of K_2H_2ppba (150 mg, 0.547 mmol) and [Cu(bpca)(H_2O)$_2$]NO_3·2H_2O (250 mg, 0.515 mmol) were placed

respectively at the bottom of the arms of a 50 mL capacity H-shaped tube. It was carefully filled with water and the arms were covered with parafilm®. The reactants were allowed to diffuse at room temperature. Deep blue prisms suitable for X-ray diffraction were grown after two months. They were collected by filtration washed with water and dried at room temperature for 48 h. Yield: 91% (220 mg, 0.234 mmol). Anal. Calcd. for $C_{34}H_{34}N_8O_{16}Cu_2$ (937.8 g mol^{-1}, **5**): C, 43.56; H, 3.62; N, 11.94; Cu, 13.40. Found: C, 43.55; H, 3.65; N, 11.95; Cu, 13.50%. IR (KBr/cm^{-1}): 3438 [ν(O–H)], 3327 [ν(N–H)], 1718 [ν(C=O)], 1676 [ν(C=O)], 1645 [ν(C=O)], 1599 [ν(C=C)], 1540 [ν(CO_2^-)], 1285 [ν(C–N)], 827 and 705 [δ (C–H)], 768 [δ (C–H)] and 488 [ν(Cu–O)].

Physical Measurements. Infrared spectra of **1**, **2**, **4** and **5** were recorded on a Perkin Elmer 882 spectrophotometer in the range of 4000 to 400 cm^{-1} using KBr pellets. NMR spectra of **1** were performed with a Bruker-200 NMR spectrometer at 200 MHz for ^{1}H nuclei and 50 MHz for ^{13}C isotope, using a mixture 4:1 dmso-d_6 and $CDCl_3$ or D_2O containing *c.a.* 50 mg of material. All spectra can be found in Supporting Information (see Figures S1-S10). Thermogravimetric analysis (TG/DTA) of **1**, **2**, **4** and **5** was done by means of a Shimadzu TG / DTA 60 equipment using *c.a.* 2.0 mg of the samples packed into an alumina crucible. The samples were heated at 10 ^{o}C min^{-1} from room temperature to 750 ^{o}C under a dynamic flow of dinitrogen (flow rate of 200 cm^3 min^{-1}). The TG/DTA curves for **1**, **2**, **4** and **5** are shown in Figures S11-S14. X-ray powder diffraction patterns for **1**, **2**, **4** and **5** were obtained using a Rigaku / Geirgeflex diffractometer at room temperature. Data were collected in the Bragg/Brentano mode (1 deg s^{-1}) using monochromatic Cu-K_α radiation (Figures S15-S18, Supporting Information). Dc magnetic susceptibility measurements were carried out on crushed crystals of **2**, **4** and **5** in the temperature range 1.9-300 K with a Quantum Design SQUID magnetometer and using applied magnetic fields of 0.1 T ($T \geq 100$ K) and 0.025

T (T < 100 K). The experimental susceptibilities were corrected by the diamagnetic corrections of the constituent atoms by using the Pascal's constants[19] [–597 (**2**), –545 (**4**) and – 570 × 10^{-6} cm^3 mol^{-1} K (**5**) per two copper(II) ions]. Corrections were also applied for the temperature-independent paramagnetism [60 x 10^{-6} cm^3 mol^{-1} per copper(II) ion] and the magnetization of the sample holder (a plastic bag).

Single crystal X-ray Diffraction. X-ray diffraction data collections were performed on an Oxford-Diffraction GEMINI diffractometer using Cu-K_α (λ = 1.5418 Å) (**2**, **4** and **5**) and Mo-K_α radiations (λ = 0.71073 Å) (**1** and **3**) at 293 (**1**, **3** and **4**), 270 (**2**) and 150 K (**5**). Data integration and scaling of the reflections for all compounds were performed with the *CRYSALIS* suite.[26] Final unit cell parameters were based on the fitting of all reflections positions. Analytical absorption corrections were performed using *CRYSALIS* suite and the space group identification was done with *XPREP*.[27] The structures of **1**–**5** were solved by direct methods using the *SUPERFLIP* program.[28] The positions of all non-hydrogen atoms for each compound could be unambiguously assigned on consecutive difference Fourier maps. Refinements were performed using SHELXL based on F^2 through full-matrix least-squares routine.[29] All non-hydrogen atoms in compounds **2**–**5** were refined with anisotropic atomic displacement parameters. Hydrogen atoms were located in difference maps and included as fixed contributions according to the riding model [U_{iso}(H) = 1.5 U_{eq}(O) for the water molecules and C–H and N–H = 0.97 Å and U_{iso}(H) = 1.2 U_{eq}(C or N) for methylene groups, aromatic carbon atoms and amide groups].[30] Spread electronic density was observed during the refinements of **2** and **4**, being associated to disordered solvent molecules, but all the attempts to model them failed (see Figures S19-S22 in Supporting Information). Squeeze technique[31] was applied for **2** and after refinement, using the new structure factors, all-residual density (78 electrons per unit cell) from the voids was removed

leaving empty cavities of *ca.* 238 Å³ in the structure. Based on elemental analysis, void volume, thermal analysis and infrared spectrum, a total of 1.33 molecules of dmf and 0.66 molecules of dmso per dicopper(II) unit was proposed to occupy the voids. This proportion of solvents per dicopper(II) unit is also in agreement with the volume occupied by the two molecules in solid state, *i.e.* 141 and 108 Å³ for the dmso and dmf molecules.[31-34] The dmso molecule in **4** could not be satisfactory modelled, and an empty void of *c.a.* 131 $Å^3$ was observed per cell unit after applying the squeeze technique, a value which is totally compatible with the molecular volume of one dmso molecule (37 electrons per unit cell supressed in the process). Hydrogen atoms of the water molecules in **5** were not assigned due to the complex water hydrogen bonding network observed. A summary of the crystal and refinement data for **1-5** are given in Table 1 whereas selected bond lengths and angles are listed in Tables S1, S2 and S3.

CCDC 1469222 (**1**), 1469225 (**2**), 1469226 (**3**), 1469223 (**4**) and 1469224 (**5**) contain the supplementary crystallographic data for this paper. The data can be obtained free of charge from The Cambridge Crystallographic Data Centre via www.ccdc.cam.ac.uk/getstructures.

RESULTS AND DISCUSSION

IR spectroscopy and thermal study. The hydrolysis of the ester groups from the Et_2H_2ppba proligand by its reaction with KOH to afford the K_2H_2ppba salt could be verified by the shift of the asymmetric C=O stretching vibrations to lower wavenumbers region from 1710 and 1685 cm^{-1} in the IR spectrum of the former species to 1675 and 1640 cm^{-1} respectively, in the latter one (Figure S1, Supporting Information). The shift of the $\nu_{C=O}$ vibrations to higher wavenumbers region at 1734 and 1656 cm^{-1}, together with the presence of a broad and strong absorption peak at 3333 cm^{-1} which is

associated to the O–H stretching mode from the carboxylic group are indicative of the formation of the neutral H_4ppba species after the hydrolysis of the Et_2H_2ppba proligand and the corresponding protonation in acid medium. In all three derivatives, the presence of a thin and strong absorption peak at 3252 (Et_2H_2ppba), 3352 (K_2H_2ppba), and 3306 cm^{-1} (H_4ppba) is attributed to the N–H stretching mode from the amide group.

A shift of the $\nu_{C=O}$ vibrations from the IR spectrum of H_4ppba to a single and broader band at 1634 cm^{-1} in that of **1** (Figure S7, Supporting Information), together with the lack of the ν_{N-H} vibration, suggest the formation of a coordinative bond with a heavy atom such as palladium after amide deprotonation. In this respect, a weak band at 523 cm^{-1} was observed in the IR spectrum of **1** which is tentatively assigned to the Pd–O vibration.[35]

The presence of the N–H stretching vibration at 3271, 3337 and 3327 cm^{-1} in the infrared spectra of **2**, **4** and **5** (Figures S8-S10, Supporting Information) respectively, supports the presence of the doubly protonated H_2ppba^{2-} ligand in these complexes. Hence, the release of the palladium(II) ions from **1** in its reaction with the $[Cu(bpca)(H_2O)_2]^+$ complex in a water/dmso/dmf solvent mixture to give **2** is accompanied by the protonation of the amidate groups of the fully deprotonated $ppba^{4-}$ species. On the other hand, the occurrence of a strong peak attributed to the C=O stretching vibration at 1717 cm^{-1} in the IR spectra of **2**, **4** and **5** is a clear diagnostic of the presence of the bpca ligand in these compounds.[17,25] Two other $\nu_{C=O}$ stretching vibrations at 1676 and 1645 cm^{-1} in their IR spectra are in turn associated to the protonated amide and carboxylate groups from the H_2ppba^{2-} ligand. In fact, these last stretching vibrations are shifted in comparison with those for Et_2H_2ppba (1734 and 1686 cm^{-1})[24] and H_4ppba (1734 and 1656 cm^{-1}), but not so much as for K_2H_2ppba (1675 and 1640 cm^{-1}), in agreement with the previous assignment of the ligand protonation

degree. Besides, the shift of the $\nu_{C=O}$ vibrations from the doubly protonated H_2ppba^{2-} ligand in the IR spectra of **2**, **4** and **5** to higher wavenumbers region when compared to that of the fully deprotonated $ppba^{4-}$ ligand in **1** (1634 cm^{-1}) suggests the occurrence of a new coordination mode to a lighter copper(II) ion. Since different crystallization solvent molecules occur in each compound of this family, some of their characteristic vibrations are observed in the IR spectrum of each solvate. So, the peak at 1025 cm^{-1} which is associated with the $\nu_{S=O}$ stretching vibration in the case of **2** and **4** reveals the presence of dmso molecules, whereas the $\nu_{C=O}$ and ν_{C-N} stretching vibrations of the dmf molecules were found at 1676 cm^{-1} (**2**), or 1651 cm^{-1} (**4**) and 1285 cm^{-1} (**2** and **4**), respectively. Finally, an intense and broad absorption centered at 3438 cm^{-1} in the IR spectrum of **5** is attributed to the ν_{O-H} stretching vibration of the water molecules.

Thermogravimetric and differential thermal analysis (TG/DTA) for **1** (see Figure S11, Supporting Information) exhibit a sequence of weight losses between 25 and 180 ºC in endothermic processes, with a combined mass loss of 4.51% that would correspond to the release of two water molecules per formula unit (calcd. 4.00%). The further weight loss occurring until 750 ºC is attributed to the decomposition of organic matter, reaching 54.20% of the initial mass as residue. TG/DTA curves for **2** (Figure S12, Supporting Information) show an endothermic weight loss of 15.85% of the initial mass between room temperature and 190 ºC, which is attributed to the release of 1.33 dmf and 0.66 dmso molecules per formula unit (calcd. 15.30%). Three other and more endothermic processes occurring between 190 and 600 ºC are accordingly assigned to the thermal decomposition of organic matter. The residue at 600 ºC corresponds to 14.74% of the initial mass and it can be associated to two mol of copper(I) oxide per mol of **2** (calcd. 14.60%).[36] An initial weight loss of 7.89% occurs in **4** between 25 and 235 ºC in a single endothermic process (Figure S13, Supporting Information), which is

associated to the release of one dmso molecule per formula unit (calcd. 8.51%). The resulting compound is thermally stable until 250 ºC, when a series of endothermic processes occur until 700 ºC, probably due to the decomposition of the ligand. The final residue corresponding to 18.94% of the initial mass probably corresponds to a copper(I/II) oxide mixture and some carbonized material, since no plateau was observed at this temperature. Finally, the analysis of the TG/DTA curves of **5** shows a first weight loss between 25 and 100 ºC in an endothermic process corresponding to 10.53% of the initial mass (Figure S14, Supporting Information), which is associated to the release of six water molecules per formula unit (calcd. 11.56%). The resulting compound is thermally stable until 285 ºC, when endothermic and exothermic processes start until 700 ºC, which are then associated to the decomposition of the ligands. The resulting residue represents 25.85% of the initial mass and since the plateau was not reached with a very high percentage, neither pure nor even phase mixtures could be proposed.

Table 1. Summary of the Crystal Data and Refinement Details for **1–5**

Compound	**1**	**2**	**3**	**4**	**5**
Formula	$C_{20}H_{16}N_4O_{16}K_4Pd_2$	$C_{34}H_{22}N_8O_{10}Cu_2$	$C_{34}H_{26}N_8O_{12}Cu_2$	$C_{34}H_{22}N_8O_{10}Cu_2$	$C_{34}H_{34}Cu_2N_8O_{16}$
Fw	910.61	829.68	865.71	829.68	937.77
T /K	293(2)	270(2)	150(2)	293(2)	150(2)
λ /Å	0.71073	1.5418	0.71073	1.5418	1.5418
Crystal system	Monoclinic	Triclinic	Monoclinic	Triclinic	Triclinic
Space group	$P2_1/n$	$P\bar{1}$	$P2_1/n$	$P\bar{1}$	$P\bar{1}$
a /Å	10.4022 (2)	9.2697 (4)	8.485 (5)	5.2579 (3)	8.895 (5)
b /Å	6.9426 (1)	9.5153 (4)	15.466 (5)	9.1706 (7)	9.145 (5)
c /Å	17.6591 (4)	13.3389 (5)	13.737 (5)	19.3079 (14)	12.690 (5)
α /°	90.0	78.365 (4)	90.0	89.809 (6)	96.274 (5)
β /°	97.571 (2)	69.696 (4)	101.566 (5)	88.898 (5)	90.087 (5)
γ / °	90	68.846 (4)	90.0	74.173 (6)	115.626 (5)
V/ Å^3	1264.19 (4)	1025.14 (7)	1766.1 (13)	895.53 (11)	923.8 (8)
Z	2	1	2	1	1
ρ / Mg m^{-3}	2.368	1.344	1.628	1.538	1.686
μ /mm^{-1}	2.17	1.80	1.28	2.06	2.19
F(000)	880	420	880	420	480
Crystal size/ mm^3	0.19 × 0.16 × 0.15	0.22 × 0.08 × 0.03	0.42 × 0.30 × 0.07	0.41 × 0.13 × 0.03	0.40 × 0.13 × 0.07
Reflections collected	18133	14998	53193	7909	26941
Goodness-of-fit on F^2	1.20	1.03	1.09	1.04	1.07
R^a, wR^b [$I > 2\sigma(I)$]	0.0275, 0.0679	0.0381, 0.0985	0.0327, 0.0826	0.0440, 0.113	0.0597, 0.1528
R^a, wR^b (all data)	0.0322, 0.00692	0.0495, 0.11044	0.0377, 0.0860	0.0588, 0.1195	0.0714, 0.1643
Larg. diff. peak and hole / e Å^{-3})	0.97, –0.48	0.32, –0.24	0.59, –0.33	0.34, –0.27	1.04, –0.72

$^a R = \Sigma \, ||F_o| - |F_c|| \, / \, \Sigma \, |F_o|$. $^b wR \, [\Sigma \, (|F_o|^2 - |F_c|^2)^2 \, / \, \Sigma \, |F_o|^2]^{1/2}$.

Description of the Structures. Crystal Structure of [{$K_4(H_2O)_2$}{$Pd_2(ppba)_2$}] (1). The structure of **1** consists of dipalladium(II) metallamacrocycle anionic entities of the [3.3] metallacyclophane type of formula $[Pd_2(ppba)_2]^{4-}$ (Figure 1) units (see Figure 1), which are further coordinated to partially hydrated potassium(I) cations through its for oxamate groups leading to a neutral 3D network (see Figure S23, Supporting Information). This compound belongs to the series of *N,N'*-1,*n*-phenylenebis(oxamate)-based palladium(II) complexes (*n* = 2-4) previously reported by some of us.[12,37] Each palladium(II) ion in **1** is four-coordinate in a square planar geometry. Similar geometry was observed for its parent compound of formula [{K_4(dmso)(H_2O)}{$Pd_2(mpba)_2$}],[12] where the coordination sphere around each palladium(II) ion has the two nitrogen atoms in *cis* positions. The values of the bond lengths [Pd–N = 2.010(3) and 2.019(3) Å; Pd–O = 2.014(2) and 2.040(2) Å] and bond angles subtended by the oxamate fragments at the palladium(II) ion [O1–Pd1–N1 = 81.63(11) and $N2^i$-Pd1-$O6^i$ = 81.36(11)°; symmetry code: (i) = –*x*+1, –*y*+1, –*z*+1] see Table S1 in Supporting Information agree with those observed in other structures of bis(oxamato)palladate(II) complexes (Pd–N = 1.99-2.04 Å, Pd–O = 1.97-2.04 Å, and N–Pd–O = 81.2-82.7°).[12,37-43] The reduced bite of the bidentate oxamate fragment is the main source of the distortion from the ideal square geometry at the palladium(II) ion which is shifted by 0.0228(16) Å from the mean basal plane defined by the N1O1$N2^iO6^i$ set of atoms.

Like in the parent compound [{K_4(dmso)(H_2O)}{$Pd_2(mpba)_2$}], intramolecular π-π stacking interactions between the aromatic rings of the $[Pd_2(ppba)_2]^{4-}$ unit occurs in **1**, the value of the centroid to centroid distance being 3.28(19) Å. Since the amide nitrogen atoms have their major resonance with the carbonyl groups rather than the aromatic rings, these last ones are not forced to be coplanar with the oxamate mean planes, but close to the orthogonality, with a value of the dihedral angle of 75.43(9)°

(see Figure 2). The mean equatorial plane at the palladium(II) ion and the oxamato fragments are practically coplanar [values of the dihedral angle of 11.42(3)º]. The intramolecular Pd1···Pd1^{i} separation across the 1,4-phenylenediamidate bridges in **1** is 8.067(2) Å, a value which is certainly longer than that through the 1,3-phenylenediamide bridges in [{K_4(dmso)(H_2O)}{Pd_2(mpba)$_2$}] [ca. 6.82 Å].[12]

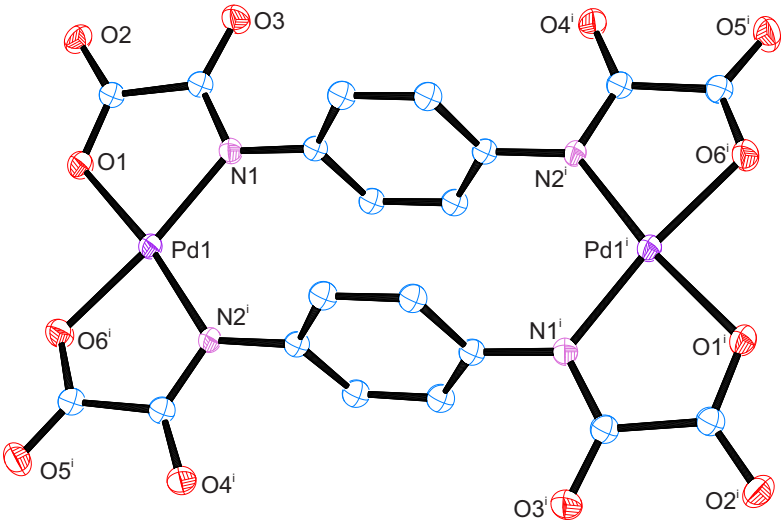

Figure 1. Perspective view of the [Pd_2(ppba)$_2$]$^{4-}$ unit of **1** showing the atom numbering of the non-carbon atoms. Hydrogen atoms were omitted for clarity. Thermal ellipsoids are drawn at the 50% probability level [symmetric code: (i) = –*x*+1, –*y*+1, –*z*+1].

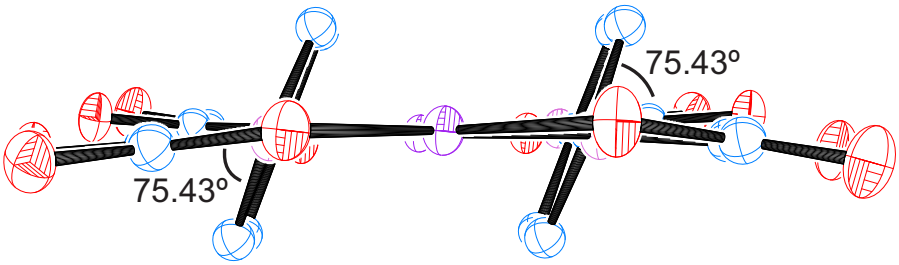

Figure 2. Side view along the palladium(II) ions of the [Pd_2(ppba)$_2$]$^{4-}$ entity showing the dihedral angle between the aromatic rings and oxamate groups. Color code: blue, red and violet stand for the carbon, oxygen and palladium atoms, respectively. Hydrogen atoms were omitted for clarity.

Two crystallographically independent potassium(I) cations (K1 and K2) occur in **1**. They are seven-coordinate in a somewhat distorted trigonal prismatic square face monocapped environment, where a water molecule (O7) and all the oxamate-oxygen atoms from the dipalladium $[Pd_2(ppba)_2]^{4-}$ are involved as donors (Figure 3). The K–$O_{oxamate}$ distances vary from 2.654(3) (K2–O6^{iv}) to 3.172 (3)Å (K2–O1^{viii}), values which are consistent with those found in other palladium(II)-oxamate complexes such as $[\{K_4(H_2O)_2(dmso)_2\}\{Pd_2(mpba)_2\}]$[12] and $[\{K_4(H_2O)_3\}$*cis*-$\{Pd(2,6\text{-}Me_2pma)_2\}_2]$ [2,6-Me_2pma = *N*-2,6-dimethylphenyloxamate][40] [K–$O_{oxamate}$ = 2.660(3)-3.084(3) Å and 2.680(2)-3.044(3) Å, respectively]. Yet the geometry around the alkaline metal ion is very different due to the high coordination number and/or the presence of ion-π interactions with the aromatic rings in **1**.

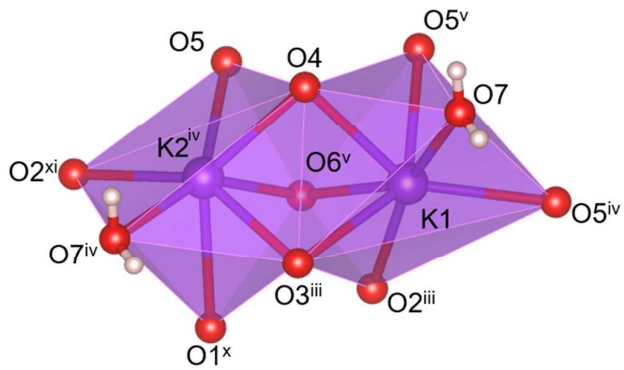

Figure 3 Coordination polyhedra for the crystallographically independent seven-coordinate K1 and K2 atoms in **1** [symmetry code: (iii) = 3/2–*x*, 1/2+*y*, 1/2–*z*; (iv) = *x*, –1+*y*, *z*; (x) = 1+*x*, 1+*y*, 1+*z*; (xi) = 3/2–*x*, 1/2+*y*, 1/2–*z*].

[{Cu(bpca)}$_2$(H$_2$ppba)·1.33dmf·0.66dmso]$_n$ (2). Compound **2** is a neutral copper(II) chain whose dinuclear repetition unit, [{Cu(bpca)}$_2$(μ-H$_2$ppba)], is constituted by two [Cu(bpca)]$^+$ cations connected by one H$_2$ppba^{2-} spacer (see Figure 4).

Each copper(II) ion in **2** is six-coordinate in a highly distorted octahedral surrounding: one amidate- (N3) and two pyridine-nitrogen atoms (N2 and N4) from the peripheral bpca$^-$ ligand and a carboxylate-oxygen atom (O2) of a monoprotonated oxamate group from the H$_2$ppba^{2-} bridging ligand occupy the equatorial positions, whereas one carbonyl-oxygen atom (O3) and one carboxylate-oxygen (O2^{ii}; symmetry code: (ii) = 2–*x*, –*y*, 1–*z*] from a symmetry related monoprotonated oxamate fragment fill the axial positions. The Cu–N$_{bpca}$ bond distances vary in the range of 1.939(2)-2.023 (2) Å, with the inner amidate bond length being shorter than the outer pyridine ones. These values agree with those reported previously for several [bis(2-pyridylcarbonyl)]copper(II) complexes.[12,17,25,44-52] The reduced bite of the two fused five-membered chelate rings subtended at the copper(II) ion by the tridentate bpca ligand accounts for the significant deviation of the values of the N2–Cu1–N3 [81.71(9)°] and N3–Cu1–N4 [82.17(9)°] bond angles from the ideal value of 90° corresponding to an octahedral surrounding. For more details about bond and angles in **2** see Table S2 in the Supporting Information.

Each monoprotonated oxamate group of the H$_2$ppba^{2-} ligand in **2** adopts the bidentate/outer monodentate bridging mode (μ-$\kappa^2 O,O':\kappa O$), leading to a di-μ-centrosymmetric oxo(carboxylate-oxamate)dicopper(II) core [Cu1O2O2^{ii}Cu1^{ii}; symmetry code (ii) = 2–*x*, –*y*, 1–*z*] with a short-long bond length alternation (Figure 5). The values of the Cu1···Cu1^{ii} distance and the angle at the bridgehead O2 atom are 3.6636(11) Å and 107.61(10)º respectively, while the intrachain Cu1···Cu1^{i} separation

though the extended H_2ppba^{2-} ligand is 12.7814(13) Å [symmetry operation: (*i*) = 2–*x*, –*y*, –*z*].

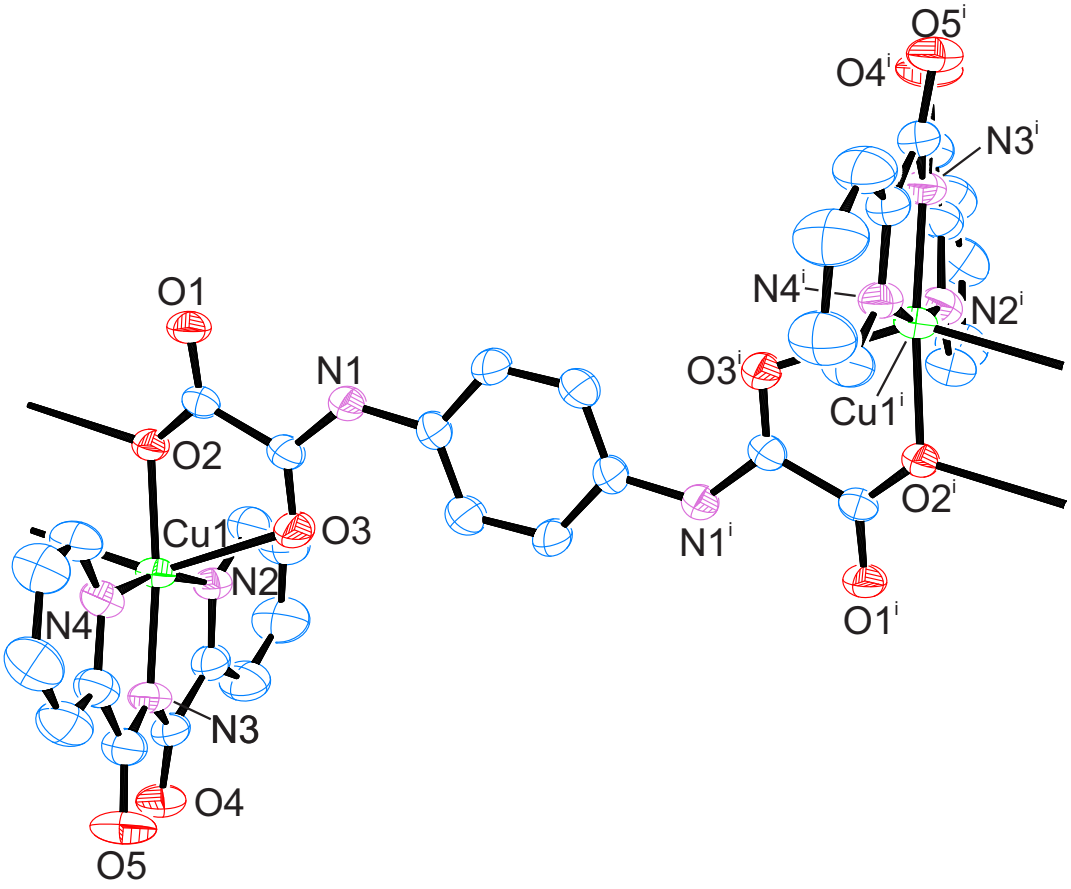

(a)

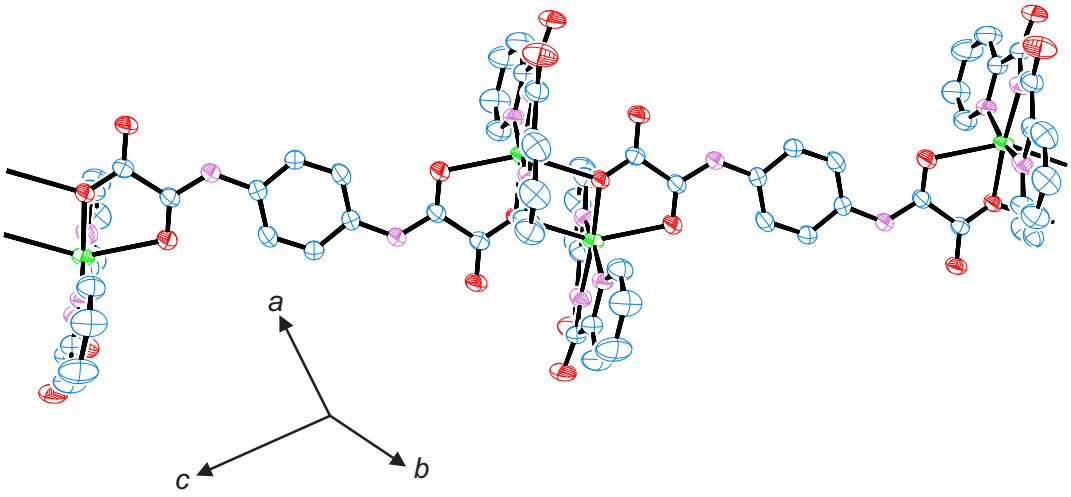

(b)

Figure 4. (a) Perspective view of the [{Cu(bpca)}$_2$(μ-H$_2$ppba)] repeating unit of **2** with the atom numbering of the non-carbon atoms. (b) View of a fragment of the chain of **2**. The thermal ellipsoids are drawn at the 50% probability level and the hydrogen atoms were omitted for clarity.

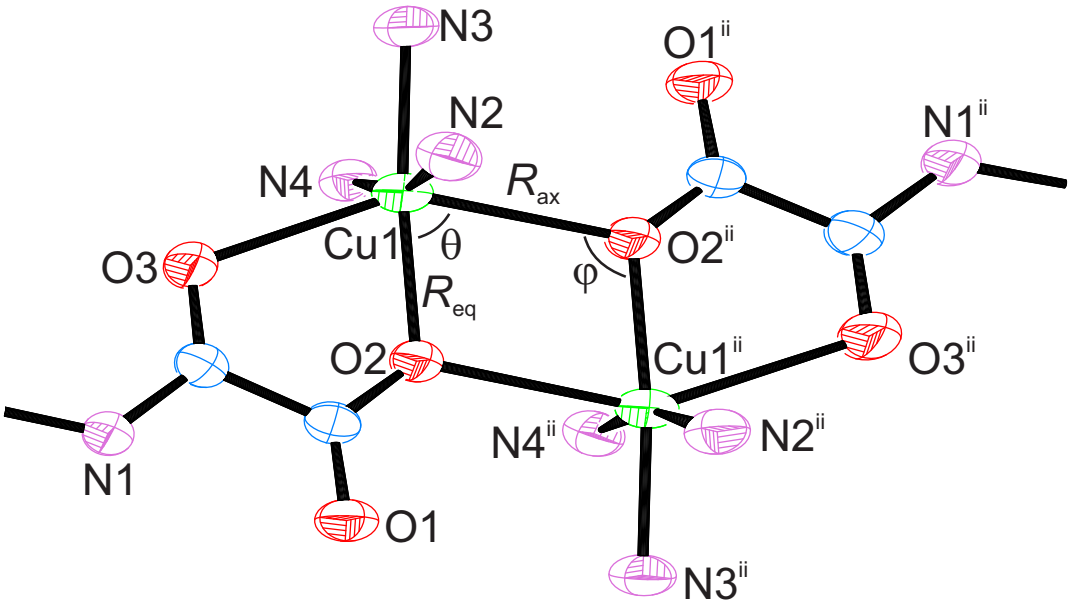

Figure 5. A detail of the double oxo(carboxylate-oxamate)dicopper(II) entity in **2**, showing the equatorial Cu1–O2 [R_{eq} = 1.964(3) Å] and axial Cu1–O2^{ii} [R_{ax} = 2.538(3) Å] bond distances and the corresponding O2–Cu1–O2^{ii} [θ = 72.39(10)º] and Cu1–O2–Cu1^{ii} [φ = 107.61(10)º] bond angles within the Cu_2O_2 core.

The neutral chains in **2** are interlinked by N-H···O and C-H···O type interactions involving amide- and phenylene-hydrogen atoms from the H$_2$ppba^{2-} bridging ligand and one of the two carbonyl-oxygen atoms from the peripheral bpca$^-$ ligand of adjacent chains, as indicated in Figure 6 [N1···O5^{iii} = 3.076(2) Å and C5···O5^{iii} = 3.193(3) Å, respectively; symmetry code: (*iii*) = 1+*x*, −1+ *y*, *z*]. In addition, the uncoordinated carboxylate-oxygen atom (O1) from the oxamato group of the H$_2$ppba^{2-} bridging ligand and the remaining carbonyl-oxygen atom (O4) from the bpca$^-$ ligand are also involved

in weak-C_{ar}–H···O type interactions with phenylene hydrogen atoms from the H_2ppba^{2-} bridging ligand leading to a supramolecular 3D network (Figure S24, Supporting Information).

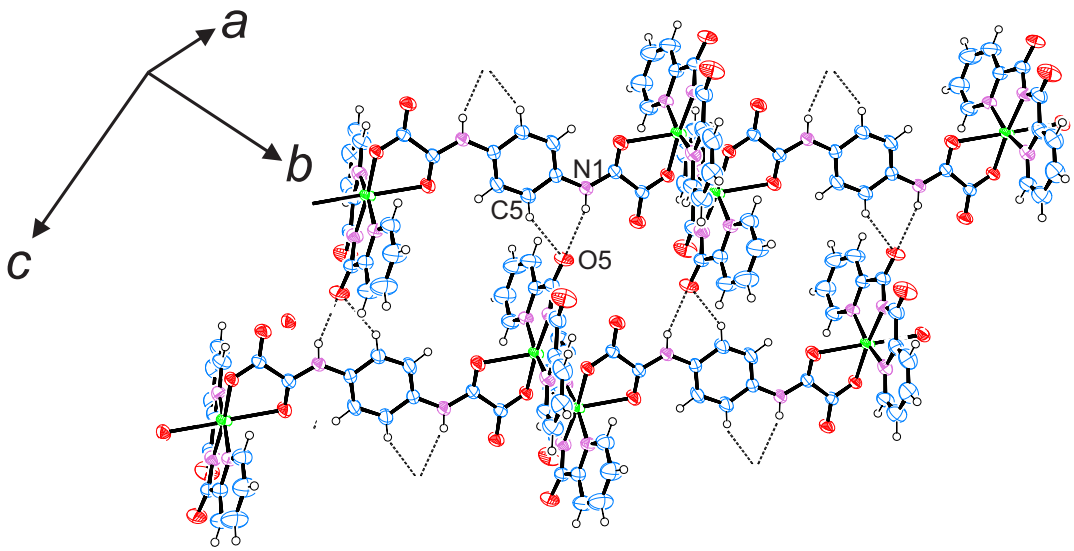

Figure 6. Perspective views of the crystal packing of adjacent chains in **2** showing the accessible voids which are occupied by crystallization solvent molecules and featuring the main N–H···O/C–H···O type interactions. Color code: blue, red, purple and green refer to carbon, oxygen, nitrogen and copper atoms, respectively.

The large cavities of approximate dimensions 7.5 × 8.7 Å (down the crystallographic *b* axis, with a volume of 238 Å³ per unit cell) occurring in the crystal packing of **2** are occupied by solvent molecules. However, neither dmf nor dmso molecules from the solvent mixture used in the synthesis, whose presence is detected by the other chemical characterizations, could be modelled in these cavities due to the spread electron density (see Experimental Section).

[{Cu(H_2O)(bpca)}$_2$(H_2ppba)] (3). Compound **3** is a neutral centrosymmetric dinuclear copper(II) complex where two peripheral [Cu(bpca)(H_2O)]$^+$ cations are linked by one H_2ppba^{2-} moiety acting as a bis(monodentate) bridging ligand (Figure 7). As far as we know, this compound constitutes the first example where the monoprotonated oxamate fragment coordinates to a transition metal ion in a monodentate fashion through the carboxylate group.

Each copper(II) ion in **3** is five-coordinate in a somewhat distorted square pyramidal surrounding: three nitrogen atoms of the bpca$^-$ ligand (N2, N3 and N4) and a carboxylate-oxygen atom (O1) from a monoprotonated oxamate fragment form the basal plane while a water molecule (O6) occupies the apical site. The value of the trigonality parameter (τ) at the metal atom is 0.0014 (τ = 0 and 1 for ideal square pyramidal and trigonal bipyramidal environments, respectively).[53] The value of the dihedral angle between the mean plane of the bpca ligand and the one of the oxamate fragment is 76.11(10)º whereas that of the oxamate fragment and the phenylene ring is 13.72(8)º. The copper-copper distance across the bis(monodentate) H_2ppba^{2-} bridging ligand is 14.452(4) Å [Cu1···Cu1^{i}; symmetry code: (i) = 3–*x*, –*y*, 1–*z*], a value which is much longer than the shortest intermolecular metal-metal separation [4.1863(11) Å for Cu1···Cu1^{ii}; symmetry code: (*ii*) = 2–*x*, –*y*, –*z*].

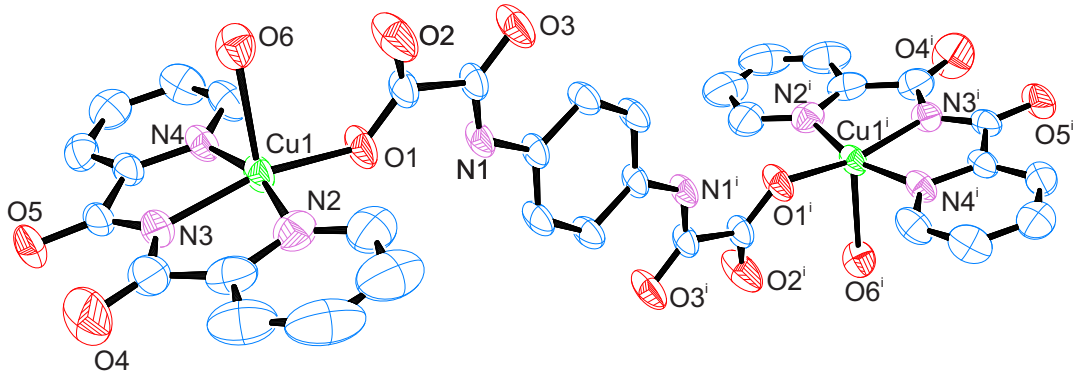

Figure 7. Perspective view of the neutral dicopper(II) entity of **3** together with the atom numbering of the non-hydrogen atoms. The hydrogen atoms were omitted for clarity and the thermal ellipsoids are drawn at the 50% probability level atom [symmetry code: (i) = 3–*x*, –*y*, 1–*z*].

The neutral dicopper(II) units in **3** are interlinked through hydrogen bonds involving the coordinated water molecule (O6), the amide-hydrogen atom (N1) and the free carboxylate-oxygen atom (O2) from the monoprotonated oxamate fragment of the H_2ppba^{2-} bridging ligand, and one of the carbonyl-oxygen atoms (O5) of the $bpca^-$ ligand (see Table 2 and Figure 8). Moreover, π-π stacking interactions occur between each pyridyl ring of the $bpca^-$ ligand and another one from two adjacent dicopper(II) units, contributing to the stabilization of the resulting supramolecular 3D network (see Figure S25, Supporting Information). The value of the centroid-centroid distance between the aromatic pyridyl rings is 3.60(6) Å and the value of the angle between centroid-centroid vector and the normal to one of the aromatic rings is 32.3(3)º.

Table 2. Hydrogen Bonds in **3**[a,b]

D–H···A	D–H / Å	H···A / Å	D···A / Å	D–H···A / deg
O6–H6*B*···O2	0.90 (2)	1.91 (2)	2.709 (3)	148 (2)
O6–H6*A*···O3[iii]	0.87 (2)	1.94 (2)	2.793 (2)	167 (3)
N1–H1···O5[iv]	0.86	2.17	2.916 (3)	145

[a]D = donor and A = acceptor. [b]Symmetry code: (iii) = *x*–1/2, –*y*+1/2, *z*–1/2; (iv) = –*x*+2, –*y*, –*z*.

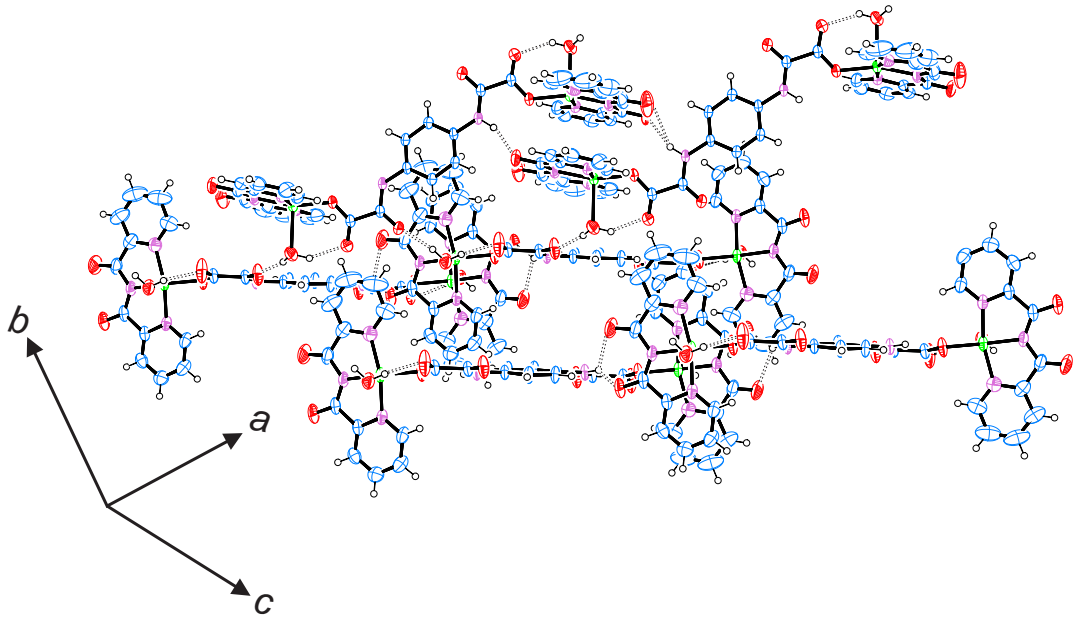

Figure 8. A view of the hydrogen bonding pattern (dotted lines) interlinking the dicopper(II) units in **3**. Color code: blue, red, purple and green stand for carbon, oxygen, nitrogen and copper atoms, respectively.

[{Cu(bpca)}$_2$(H$_2$ppba)]·dmso (4) and [{Cu(bpca)}$_2$(H$_2$ppba)]·6H$_2$O (5). The structures of **4** and **5** consist of neutral centrosymmetric dicopper(II) units, [{Cu(bpca)}$_2$(H$_2$ppba)], where two terminal [Cu(bpca)]$^+$ cations are connected by a bis(bidentate) H$_2$ppba^{2-} ligand (Figure 9), together with non-coordinated dmso (**4**) and water molecules (**5**).

Each copper(II) ion in **4** and **5** is five-coordinate in a somewhat distorted square pyramidal surrounding formed by three nitrogen atoms of the capping bpca$^-$ ligand (N2, N3 and N4) and a carboxylate-oxygen atom (O2) from a monoprotonated oxamate fragment of the H$_2$ppba^{2-} bridging ligand in the basal plane, while the carbonyl-oxygen atom (O3) occupy the apical site. The values of τ are 0.252 (**4**) and 0.280 (**5**) indicating a similar distortion of the metal environment in both solvates. The main contribution to

this distortion is caused by the reduced bite of the bidentate monoprotonated oxamate ligand. In this respect, the values of the O2–Cu1–O3 angle of 77.41(9) (**4**) and 79.51(14)º (**5**) differing by *ca.* 13º and *ca.* 11º from the ideal value of 90°. The dihedral angle between the mean plane of the bpca ligand and the oxamate fragment is close to the orthogonality [76.27(6)º and 77.76(5)º in **4** and **5**, respectively]. The values of the copper-copper separation through the bis(bidentate) H_2ppba^{2-} bridging ligand are 12.8452(13) Å (**4**) and 12.394(4) Å (**5**) [Cu1···Cu1^{i}; (i) = –*x*+1, –*y*+2, –*z*+1 (**4**) and (i) = 2–*x*, 2–*y*, –*z* (**5**)]. They are somewhat shorter than that across the bis(monodentate) H_2ppba^{2-} bridging ligand in **3** [14.452(4) Å] but much longer than the shortest intermolecular metal-metal separations, 5.2579(3) (**4**) and 6.242(3) Å (**5**) [Cu1···Cu1^{ii}; (ii) = 1+*x*, *y*, *z* (**4**) and (ii) = 1–*x*, 2–*y*, –*z* (**5**)]. For more details of the copper environment for **4** and **5** see Table S3 in Supporting Information.

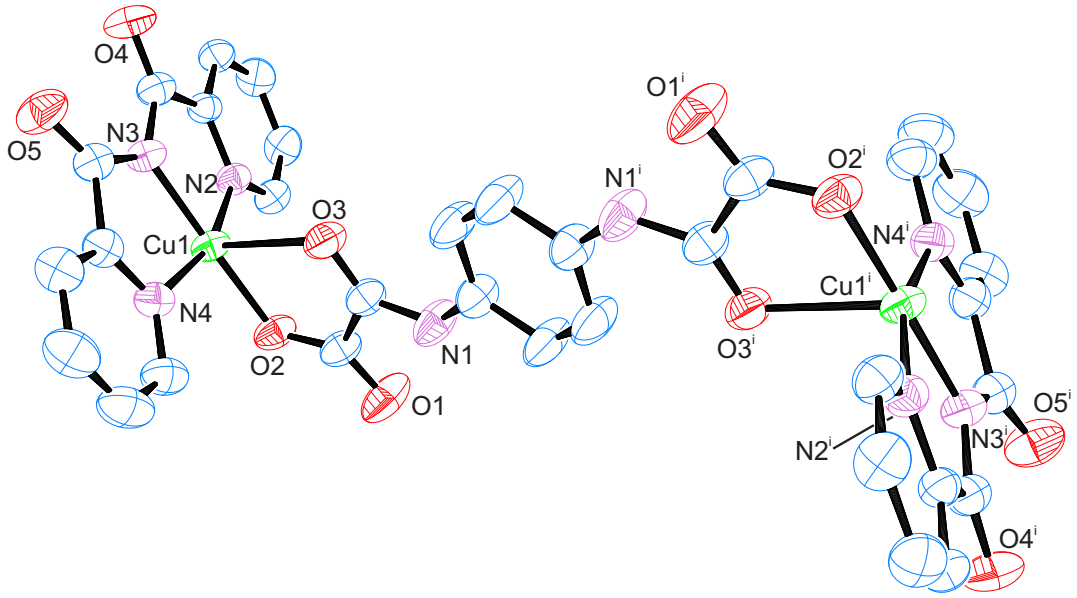

(a)

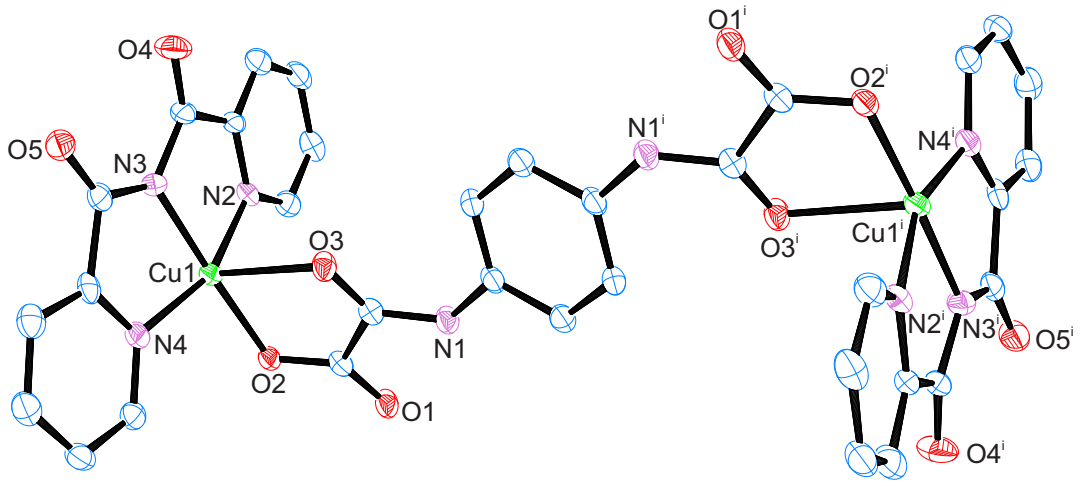

(b)

Figure 9. Perspective views of the neutral dicopper(II) unit in **4** (a) and **5** (b) with the atom numbering of the non-carbon atoms. Hydrogen atoms were omitted for clarity. Thermal ellipsoids are drawn at the 50% probability level [symmetry code: (i) = –*x*+1, –*y*+2, –*z*+1 (**4**) and (i) = 2–*x*, 2–*y*, –*z* (**5**)].

The voids in the crystal packing of **4** and **5** are filled by the crystallization dmso (**4**) and water molecules (**5**). The free dmso molecules interact weakly with the dicopper(II) units in **4**, when compared to the interactions (π-π stacking and dipole-dipole) among the adjacent dicopper(II) units which rules the crystal packing. This can be confirmed by the spread electronic density in the voids of **4** (see Figures S21 and S22, Supporting information), which would eventually result from the combination of all possible positions of the dmso molecule in the asymmetric unit without influencing the packing of the dicopper(II) units. The six crystallization water molecules per dicopper(II) unit in **5** occupy the free space of the voids and they contribute to the crystal packing interacting among themselves and also with the dicopper(II) units by means of hydrogen bonds.

More likely, as a result of the different nature of the solvent molecules in **4** and **5**, the better crystal packing of the dicopper(II) units is reached through distinct conformations of the H_2ppba^{2-} bridging ligand. Hence, the values of the dihedral angle between the mean planes of the phenylene ring and the monoprotonated oxamate fragment are 10.63(25) (**4**) and 28.19(30)º (**5**). On the other hand, no N–H···O type hydrogen bonds are observed in **4**, but they are present in **5** [N1···O1^{iii} = 2.926(6) Å and N1–H1···O1^{iii} = 130.5º; symmetry code: (iii) = 2–*x*, 1–*y*, –*z*]. These hydrogen bonding interactions in **5** occur in the double symmetrical form, where two oxamate groups interact via a pair of N–H···O hydrogen bonds (Figure 10), as previously observed in several examples of protonated amide-oxamate groups where the amide-hydrogen atom interacts with one carboxylate-oxygen.[54–58] A weak C_{ar}–H···O type interaction between one hydrogen atom (H14) from a pyridyl ring of the $bpca^{-}$ ligand of one dicopper(II) unit and the coordinated carbonyl-oxygen atom (O3^{iv}) from a monoprotonated oxamate fragment of the H_2ppba^{2-} bridging ligand of a close dicopper(II) unit was also observed

in **5** [C14···O3^{iv} = 3.158(7) Å and C14-H14···O3^{iv} = 140.0º; symmetry code: (iv) = 2–*x*, 2–*y*, 1–*z*], together with other weak C_{ar}–H···O contacts between the hydrogen atoms from the pyridyl rings (H16 and H17) and one carbonyl-oxygen atom (O4^{v}) [symmetry code: (v) = 1+*x*, *y*, *z*] of the bpca ligands from adjacent dicopper(II) units (see Table 3). Also, out-of-plane Cu···O_{bpca} contacts were observed in these structures, helping in their crystal packing. The values of the weak interaction distance are 3.102(3) Å for **4** [Cu1···O4^{v}, (*v*) = 1–*x*, –*y*, –*z*] and 4.034(3) Å for **5** [Cu1···O4^{vi}, (*vi*) = 1–*x*, 2–*y*, –*z*].

Table 3. Selected Intermolecular Interactions in **5**[a,b]

D–H···*A*	D–H / Å	H···A / Å	D···A / Å	D–H···*A* / deg
N1–H1···O1^{iii}	0.86	2.29	2.926 (6)	131
C16–H16···O4^{v}	0.93	2.59	3.088 (7)	114
C17–H17···O4^{v}	0.93	2.35	2.984 (7)	125
C14–H14···O3^{iv}	0.93	2.39	3.158 (7)	140

[a]D = donor and A = acceptor. [b]Symmetry code: (iii) = 2–*x*, 1–*y*, –*z*; *iv* = 2–*x*, 2–*y*, 1–*z*; *v* = 1+*x*, *y*, *z*.

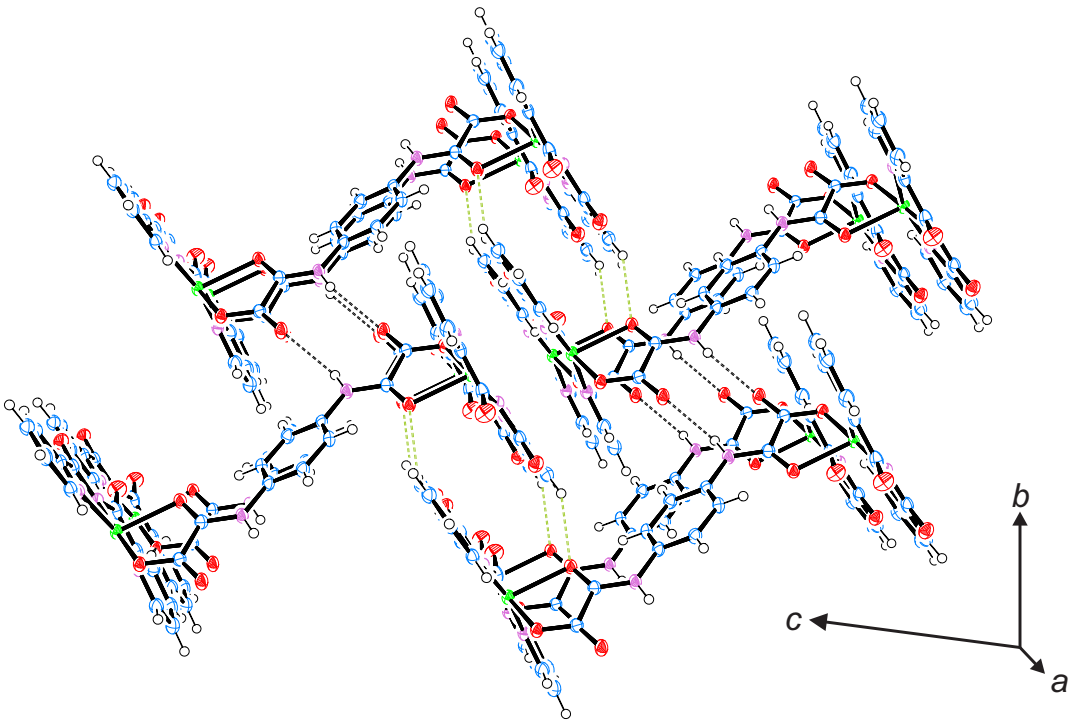

Figure 10. A view of the crystal packing in **5** showing the double symmetrical N–H···O hydrogen bonds (black dots) and the C_{ar}–H···O type interactions (lime green dot lines). Color code: carbon in blue, red, purple and greens refer to carbon, oxygen, nitrogen and copper.

Comparison of crystal structures. Among the presented crystal structures, **2**, **3**, **4** and **5** have very similar composition, consisting of two $[Cu(bpca)]^+$ units linked by the H_2ppba^{2-} spacer. **2**, **4** and **5** share the $[\{Cu(bpca)\}_2\{H_2ppba\}]$ entity which is solvated (per unit), by 1.33dmf and 0.66dmso, one dmso molecule and six water molecules, respectively. Besides the similarities in the composition, they feature very different structural properties. The $[\{Cu(bpca)\}_2\{H_2ppba\}]$ units in **2** are interlinked by double oxo(carboxylate)-oxamate bridges forming a Cu_2O_2 core and leading to a 1D coordination polymer, meanwhile **4** and **5** are built up by discrete units. The major differences concerning their structures resides in the conformation of free to rotate bonds, such as the N–C_{ar}, or the torsion in the $bpca^-$ ligand (see Figure S26 in the Supporting Information). In contrast, the crystal structure of **3** shows the H_2ppba^{2-} ligand linking the metal ions in a bis-monodentate form letting one water molecule to coordinate to each copper(II) ion of the discrete $[\{Cu(bpca)\}_2\{H_2ppba\}]$ unit.

Influence of the palladium(II) ion and the solvent in the synthesis of the complexes

Our previous attempts to obtain oxamate-bridged heterobimetallic copper(II)-palladium(II) systems afforded the tri- and hexanuclear complexes of formula $[\{Cu(bpca)\}_2\{Pd(opba)\}]\cdot1.75dmso.0.25H_2O$ and $[\{Cu(bpca)\}_4\{Pd_2(mpba)_2\}]\cdot6H_2O$, respectively.[12] When using the $[Pd_2(ppba)_2]^{4-}$ unit as metalloligand *versus* the $[Cu(bpca)(H_2O)_2]^+$ cationic complex, however, single crystals of the envisaged

complexes of formula $[\{Cu(bpca)\}_x\{Pd_2(ppba)_2\}]$ ($1 \leq x \leq 4$) were not obtained, whereby the $ppba^{4-}$ would act as either bridging bis-bidentate μ-$\kappa^2N,O:\kappa^2N',O'$ or bridging tetrakis-bidentate μ_4-$\kappa^2N,O:\kappa^2O',O'':\kappa^2N',O''':\kappa^2O^{iv},O^{v}$ (see Schemes 3a and 3b, respectively). The palladium(II) ion was released by its ligand and the $[\{Cu(bpca)\}_2(H_2ppba)]$ moieties were formed instead. Most likely, the partial protonation of the $ppba^{4-}$ ligand occurs because of the high pK_a value of the amide group (values of pH greater than 11.0 are required to deprotonate the oxamide group from *N*-substituted oxamides),[15] and it only goes down when the coordination to a metal ion such as Pd^{II} or Cu^{II} takes place in the presence of a base, as illustrated by the formation of complexes such as $[Pd(opba)]^{2-}$,[12,37,38] $[Pd_2(mpba)_2]^{4-}$,[12] $[Cu_2(edpba)_2]^{4-}$,[16] or $[Cu(opba)]^{2-}$.[59]

(a)

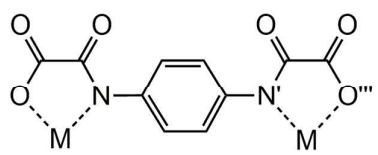

μ-$\kappa^2N,O:\kappa^2N',O'$

(b)

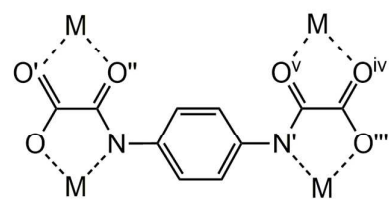

μ_4-$\kappa^2N,O:\kappa^2O',O'':\kappa^2N',O''':\kappa^2O^{iv},O^{v}$

(c)

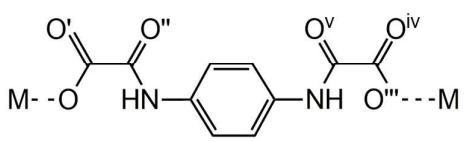

μ-$\kappa O:\kappa O'''$

(d)

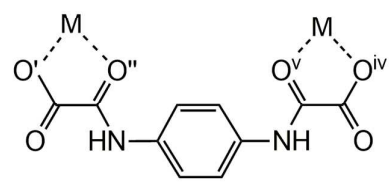

μ-$\kappa^2O',O'':\kappa^2O^{iv},O^{v}$

(e)

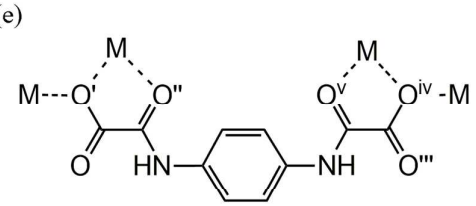

μ-$\kappa^2O',O'':\kappa O':\kappa^2O^{iv},O^{v}:\kappa O^{iv}$

Scheme 3. Coordination modes of the bridging $ppba^{4-}$ ((a) and (b)) and H_2ppba^{2-} ((c), (d) and (e)) ligands.

In the reactions involving the oxamate-containing palladium(II) complex $[Pd_2(ppba)_2]^{4-}$ as metalloligand in either a water-dmso-dmf mixture or water as solvents two different compounds were obtained, namely **2** and **3**, respectively. Compound **2** is a 1D coordination polymer where the H_2ppba^{2-} ligand adopts a μ-$\kappa^2O',O'':\kappa O':\kappa^2O^{iv},O^{v}:\kappa O^{iv}$ bridging mode (see Scheme 3e) whereas compound **3** is a discrete dinuclear complex formed by two $[Cu(bpca)]^+$ units connected by a H_2ppba^{2-} ligand exhibiting the rare bis-monodentate μ-$\kappa O:\kappa O'''$ bridging mode (see Scheme 3c). The unidentate coordination of the monoprotonated oxamate was observed previously in the dinuclear complex $[Cu(bipy)(H_2mpba)]_2 \cdot 2H_2O$[18] and in the mononuclear species $[Co(tren)(NH_3)(OOCCONH_2)]Cl_2$ [tren = tris(2-aminoethyl)amine and $HOOCCONH_2$ = oxamic acid].[60] However, in contrast to **3**, a great twisting of the unidentate monoprotonated oxamate occurs in the first example [the value of the dihedral angle between its carboxylate and amide units being 80.78(32)º][18] and the substitution of a coordinated chloride anion from the starting six-coordinate cobalt(III) complex *p*-$[Co(tren)(NH_3)Cl]^{2+}$ by the oxamate anion leads to the second example.[60]

In order to better understand this process, we tried to obtain **2** and **3** without using the dipalladium(II)-oxamate complex as precursor. The reactions of complex formation were carried out in the presence of the oxamato ligand in soluble forms, that is using either H_4ppba in water-dmso-dmf solvent mixtures or K_2H_2ppba in water. Compound **2** was obtained in a good yield by using H_4ppba instead of **1** in water-dmso-dmf solvent mixtures. Then, the desired copper(II) complex was obtained and the palladium(II) complex $[Pd_2(ppba)_2]^{4-}$ was found to be unnecessary for the synthesis of **2**. A possible explanation for the obtention of **2** by using the dipalladate(II)-oxamate

complex as metalloligand resides in the fact that the interaction between dmso and palladium(II) is favored because of the soft character of the Pd^{II} and dmso as Lewis acid and base (Pd···S), respectively. The nature of this interaction would cause the partial release of the palladium(II) ion with the subsequent protonation of the two amidate groups of the free bis-oxamate ligand, leading to the H_2ppba^{2-} anion, which in the presence of the $[Cu(bpca)]^+$ unit would afford the low-solubility neutral dicopper(II) species **2**. This suggestion is supported by the low yield of crystals of **2** when using $[Pd_2(ppba)_2]^{4-}$ as precursor which is accompanied by the formation of a main product as a green powder. The preliminary analysis of this powder is consistent with formulas like $K_{4-x}[\{Cu(bpca)\}_x\{Pd_2(ppba)_2\}]$ ($1 \leq x \leq 4$) and/or $K_{2-y}[\{Cu(bpca)\}_y\{Pd(H_2ppba)_2\}]$ ($0 \leq y \leq 2$).

A second attempt to prepare compound **2** consisted of checking the influence of each solvent in the reaction mixture. Compound **4** was then obtained by the reaction between H_4ppba and $[Cu(bpca)]^+$ in a dmso-water mixture as solvent. Its structure consists of discrete $[\{Cu(bpca)\}_2(H_2ppba)]$ entities where the H_2ppba^{2-} ligand adopts a bis-bidentate $\kappa^2O',O'':\kappa^2O^{iv},O^{v}$ bridging mode (see Scheme 3d), suggesting thus that dmf plays a key role in the synthesis of **2**. Other tests without water or dmso, but keeping the dmf did not afforded single crystals of **2** and the chemical analysis of the resulting precipitate revealed its inconsistency with any compound described in this work. Having this in mind, one can conclude that dmso is important for i) the release of the palladium(II) in the tests carried out by using **1** and ii) maintaining the different solvent phases separated in the beginning of crystallization process in both reactions using the Pd^{II} complex or H_4ppba, meanwhile the dmf is, somehow, the responsible for the proper packing of $[\{Cu(bpca)\}_2(H_2ppba)]$ entities that leads to the 1D coordination polymer observed in the crystal structure of **2**.

Finally, the attempt to prepare compound **3** by replacing **1** with K_2H_2ppba in water leads to the formation of **5** where the H_2ppba^{2-} ligand adopts the same coordination mode found in **4** (Scheme 3d). In this respect, another attempt was carried out by allowing the $[Cu_2(ppba)_2]^{4-}$ precursor instead of **1** to react with $[Cu(bpca)]^+$ in water. This synthetic pathway produced only dark green powders of general formula $A_{4-x}[\{Cu(bpca)\}_x\{Cu_2(ppba)_2\}]$ (A is a univalent cation and $1 \leq x \leq 4$). These results strongly suggest the need for the $[Pd_2(ppba)_2]^{4-}$ species in the reaction leading to the formation of **3**. Indeed, this formation could be explained by the approximation between the solvated $[Cu(bpca)(H_2O)_x]^+$ units and $[Pd_2(ppba)_2]^{4-}$ anions. Unlike in **2**, there is no solvent molecules that can do a better interaction with palladium(II) ions, compared with $ppba^{4-}$ donor atoms, to coordinate them and consequently, to make possible the removal of part of the palladium(II) ions from the oxamate complex. Thus, these results suggest that the reaction occurs between the initial complexes and not with partially degraded species.

Magnetic properties

The magnetic properties of **2**, **4** and **5** under the form of the $\chi_M T$ versus T plots [χ_M being the molar magnetic susceptibility per two copper(II) ions] are shown in Figure 11. At room temperature, the $\chi_M T$ values of 0.80 (**2**), 0.82 (**4**) and 0.76 (**5**) cm^3 mol^{-1} K are as expected for two magnetically non-interacting copper(II) ions ($\chi_M T$ = 0.83 cm^3 mol^{-1} K, with S_{Cu} = 1/2 and g = 2.1). Upon cooling, $\chi_M T$ for **2** follows a Curie law until 40 K and it further increases to reach a $\chi_M T$ value of 0.87 cm^3 mol^{-1} K at 1.9 K. This shape is typical of a weak ferromagnetic interaction between copper(II) ions. In contrast, $\chi_M T$ for **4** and **5** follows a Curie law between room temperature until *ca.* 50 K and it further decreases to attain values of 0.72 (**4**) and 0.67 cm^3 mol^{-1} K (**5**) at 1.9 K.

These different magnetic behaviors are indicative of the occurrence of weak either ferro- (**2**) or antiferromagnetic interactions (**4** and **5**) between the copper(II) ions.

Looking at the structure of the chain compound **2**, two intrachain exchange pathways could be involved: (i) the double oxo(carboxylate-oxamate) bridge and (ii) the extended H_2ppba^{2-} bridging ligand, with copper-copper distances of *ca*. 3.66 and 12.78 Å, respectively. However, the very large intermetallic separation through the (ii) pathway, allow us to discard it and then, to keep the first one as the only pathway responsible for the weak ferromagnetic coupling observed experimentally. Consequently, the magnetic data of **2** were analysed through a simple Bleaney-Bowers expression for a pair of copper(II) ions [eq (1)][19,62]

$$\chi_M T = \left(2\frac{N\beta^2 g^2}{k}\right)\left[3 + exp\left(-\frac{J}{kT}\right)\right]^{-1} \quad (1)$$

the spin Hamiltonian being defined by eq (2)

$$\boldsymbol{H} = -J(\boldsymbol{S_1}\cdot\boldsymbol{S_2}) + \beta H(g_{Cu1}\boldsymbol{S}_{Cu1} + g_{Cu2}\boldsymbol{S}_{Cu2}) \quad (2)$$

where J is the magnetic coupling parameter, g is the average Landé factor of the copper(II) ions ($g = g_{Cu1} = g_{Cu2}$) and N, β and k have their usual meanings. Least-squares best-fit parameters for **2** are $J = +0.70(1)$ cm^{-1} and $g = 2.06(1)$ with $R = 4.4 \times 10^{-5}$ (R is the agreement factor defined as $\Sigma[(\chi_M T_{obs})-(\chi_M T_{calc})]^2/\Sigma[(\chi_M T_{obs})]^2$). The theoretical curve matches very well the experimental magnetic data in the whole temperature range explored.

The use of the same approach to treat the magnetic data of the dinuclear compounds **4** and **5** led to the following best-fit parameters: $J = -0.90(1)$ cm^{-1}, and $g = 2.09(1)$ for **4** and $J = -0.79(1)$ cm^{-1}, $g = 2.01(1)$ for **5** with $R = 2.9 \times 10^{-5}$ (**4**) and 7.1×10^{-5} (**5**). These J values for **4** and **5** have to be considered with caution. In fact, given the large values of copper(II)-copper(II) separation across the extended bis-bidentate H_2ppba^{2-} ligand [ca. 12.84 (**4**) and 12.39 Å (**5**)] and the much shorter intermolecular

metal-metal distances [ca. 5.25 (**4**) and 6.24 Å (**5**)], these J values would be the upper limit for the intramolecular magnetic coupling. An alternative fit of the magnetic susceptibility data of **4** and **5** by the Curie-Weiss law of eq (3)

$$\chi_M = N\beta^2 g^2/2k_B(T - \theta) \qquad (3)$$

which only takes into account the occurrence of very weak intermolecular magnetic interactions among dicopper units, leads to the following best-fit parameters: θ = –0.35(1) K and g = 2.09(1) with $R = 4.9 \times 10^{-5}$ for **4** and θ = –0.45(1) K and g = 2.01(1) with $R = 2.5 \times 10^{-5}$ for **5**.

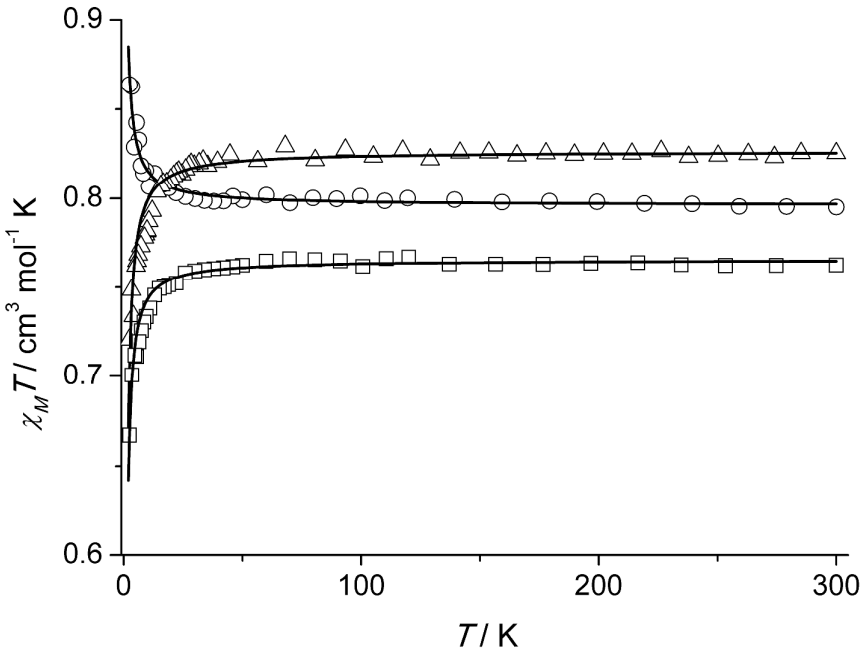

Figure 11. $\chi_M T$ against T plot for **2** (○), **4** (Δ) and **5** (□). The solid lines are the best-fit curves through eq (2) (see text).

Let us finish this work with a brief discussion about the magnitude and nature of the magnetic couplings observed in **2**, **4** and **5**. The magnetic interaction between Cu1 and Cu1^{i} in **2** is mediated through the out-of-plane exchange pathway provided by the double oxo (carboxylate)-oxamate bridge connecting one equatorial position at one

copper(II) ion with the apical site at the adjacent copper(II) ion. The unpaired electron at each copper(II) ion is defined by a $d_{x^2-y^2}$ type magnetic orbital which is delocalized in the equatorial plane (the *x* and *y* axes corresponding roughly to the Cu-N_{bpca} bonds). Then, the spin density at the copper(II) ions is mostly located in their basal planes which in turn are parallel to each other and connected in an equatorial-axial way. Under these conditions a poor orbital overlap between the two magnetic orbitals is predicted and therefore a weak magnetic coupling is expected, either ferro- or antiferromagnetic. This coupling can be ferromagnetic in the case of strict or accidental orthogonality, depending on structural factors such as the angle at the bridgehead atom (θ). Such a situation has been discussed in previous examples with di-μ-O-carboxylate,[63–65] di-μ-chloro,[66,67] di-μ-azido/cyanato,[68–70] and di-μ-oximato[71] dicopper(II) complexes, in which the nature and magnitude of the interaction depend basically on the axial Cu–X bond length (R_{ax}) and Cu–X–Cu bond angle (X = O, N and Cl). Taking into account the results in the present work together with those of related examples from the literature it is also possible to extend the analysis of relationship between the magnetic coupling and the structural parameters θ and R_{ax} to the di-μ-O-carboxylate(oxamate) dicopper(II)-family, as shown in Table 4. One can see therein that in general the antiferromagnetic interactions are found for the dicopper(II) units with the smaller values of the θ angle and also that the magnetic interactions are either ferro- or antiferromagnetic but always weak, as expected.

Table 4. Selected Magneto-Structural Data for Double Oxo(carboxylate)-Oxamate Bridged Dicopper(II) Complexes

Compound[a]	R_{ax} / Å	θ / °	J / cm^{-1}	Ref.
2	2.538(2)	107.6(1)	+ 0.70	This work
$\{[Cu(bpca)]_2(H_2opba)\}_2\cdot 6H_2O$	2.670(2)	102.8(1)	– 2.36	17
$\{[Cu(H_2edpba)(EtOH)]_2\}\cdot 2EtOH$	2.365(5)	102.7(1)	+ 2.93	17
$Na_2(C_{14}H_{12}N_2)\{[Cu(opba)]_2\}\cdot 6H_2O$	2.788(4)	95.4(1)	– 0.80	72
$(edap)_2[\{Cu(opba)\}_2]\cdot 4H_2O$	2.592(2)	96.1(1)	–1.63	73
$(edap)[\{Na_2(H_2O)_4\}\{Cu_2(opba)_2\}]\cdot 2H_2O$	2.616(1)	93.7(7)	–2.29	73
$(edap)[\{K_2(H_2O)_2\}\{Cu_2(opba)_2\}]\cdot 3H_2O$	2.911(1)	85.9(1)	–1.65	73

[a]$C_{14}H_{12}N_2$ = 6,7-dihydrodipyrido(1,2-a:2',1'-c)pyrazinium and edap = 1,2-bis(4-aminopyridinium)ethane.

Concerning the very weak antiferromagnetic coupling observed in **4** and **5**, it would correspond to the sum of both intra- and intermolecular interactions and in the light of the good fit of **2**, one can assume that the intermolecular pathways in **4** and **5** would play the main role in mediating electronic effects. Finally, it should be mentioned that a moderate to strong antiferromagnetic coupling across the ppba^{4-} ligand have been reported in their corresponding di- and tetranuclear copper(II) complexes respectively (Schemes 2a and 2b), due to the occurrence of either σ- or π-exchange pathways through the *para*-phenylenediamidate N-(C_6H_4)-N bridge.[74,75] However, the longer (O=C)NH-(C_6H_4)-NH(C=O) bridging pathway across the H_2ppba^{2-} spacer in **4** and **5** where a very weak spin density, if any, is expected for the amide nitrogen of each monoprotonated oxamate fragment (see Scheme 3d) would cause a drastic reduction of the magnetic coupling between the copper(II) ions, as observed experimentally.

CONCLUSIONS

In this work, four new copper(II) complexes (**2**–**5**) with the $bpca^{-}$ and H_2ppba^{2-} as blocking and spacer ligands were prepared and magneto-structurally characterized. Two of them (**2** and **3**), were observed from the attempts to use as the corresponding dipalladium(II)-ppba complex (**1**) as metalloligand toward the preformed $[Cu(bpca)]^{+}$ species envisaging the preparation of the heterobimetallic $[\{Cu(bpca)\}_4\{Pd_2(ppba)_2\}]$ complex. The release of the Pd^{II} ions and the partial protonation of the $ppba^{4-}$ ligand to generate the deprotonated H_2ppba^{2-} species account for the formation of **2** and **3**. The other two compounds (**4** and **5**) were obtained in our attempts to prepare **2** and **3** directly [without the palladium(II) ion] by using different solvents in their synthetic pathways. Besides the similar contents of **2**-**5**, being build up by $[\{Cu(bpca)\}_2(H_2ppba)]$ units, the crystal structures are quite different, which lead to distinct magnetic behaviours. The structures of **1**–**5** allowed us to evidence the distinct role played by the dmf solvent and $[Pd_2(ppba)_2]^{2-}$ ion to synthesize **2** and **3**, respectively. In the preparation of **2** by using **1** as the H_2ppba^{2-} source, the dmso solvent plays an important role as well. The magnetic properties of **2**, **4** and **5** revealed the occurrence of a weak intramolecular ferromagnetic coupling in **2** and very weak (likely intermolecular) antiferromagnetic interactions in **4** and **5**. The results presented here illustrate the relevance played by several factors such as the solvent, type of precursors and metal ions, etc., in the crystal engineering of polynuclear compounds which were further able to translate into different magnetic properties.

ASSOCIATED CONTENT

Supporting Information

IR spectra for Et_2H_2ppba, H_4ppba and K_2H_2ppba (Figure S1), 1H and ^{13}C NMR spectra for Et_2H_2ppba and H_4ppba (Figures S2-S5), ^{1}H NMR spectrum for **1** (Figure S6), IR spectra, X-ray powder diffraction patterns, and TG/DTA plots and crystallographic drawings for **1**, **2**, **4** and **5** (Figures S19-S26), main bond lengths and angles for **1-5** (Tables S1-S3). This material is available free of charge on the ACS Publications website at DOI: 10.1021/acs.cgd.XXXXXX.

AUTHOR INFORMATION

Corresponding Author

*E-mail: cynthialopes@ufmg.br

Notes

The authors declare no competing financial interests.

ACKNOWLEDGMENTS

Financial support from CAPES, CNPq and FAPEMIG (Brazil), Ministerio Español de Economía y Competitividad (Projects CTQ-2013-44844P and Unidades de Excelencia María de Maetzu MDM-2015-0538) and the Brazilian-Spanish Project HB2014-00024 is gratefully acknowledged. W.X.C. Oliveira and C.L.M. Pereira are grateful to CNPq for all fellowships. Authors are grateful to Dr. Rafael Ruiz-García, from Universitat de València for fruitful discussions.

REFERENCES

(1) Braga, D.; *Chem. Commun.* **2003**, 2751−2754.

(2) Lehn, J. M. *Supramolecular Chemistry, Concepts and Perspectives*, Wiley-VCH: Weinheim, 1995.

(3) Desiraju, G. R. *Crystal Engineering, the Design of Organic Solids*; Elsevier: Amsterdam, 1989.

(4) Leong, W. L.; Vittal, J. J. *Chem. Rev*. **2011**, *111*, 688−764.

(5) Dhers, S.; Feltham, H. L. C.; Brooker, S.; *Coord. Chem. Rev.* **2015**, *296*, 24−44.

(6) Li, C. P.; Du, M., *Chem. Commun.* **2011**, *47*, 5958−5972 and references therein.

(7) Kahn, O.; Larionova, J.; Yakhmi, J. V. *Chem. –Eur. J.* **1999**, *5*, 3442−2339.

(8) Grancha, T.; Ferrando-Soria, J.; Zhou, H.-C.; Gascon, J.; Seoane, B.; Pasán, J.; Fabelo, O.; Julve, M.; Pardo, E. *Angew. Chem. Int. Ed.* **2015**, *54*, 6521–6525.

(9) do Pim, W. D.; de Faria, E. N.; Oliveira, W. X. C.; Pinheiro, C. B.; Nunes, W. C.; Cano, J.; Lloret, F.; Julve, M.; Stumpf, H. O.; Pereira, C. L. M. *Dalton Trans.* **2015**, *44*, 10939−10942.

(10) do Pim, W. D.; Simões, T. R. G.; Oliveira, W. X. C.; Fernandes, I. R. A.; Pinheiro, C.B.; Lloret, F.; Julve, M.; Stumpf, H. O.; Pereira, C. L. M. *Crystal Growth & Design* **2014**, *14*, 5929−5937.

(11) Marinho, M. V.; Simões, T. R. G.; Ribeiro, M. A.; Pereira, C. L. M.; Machado, F. C.; Pinheiro, C. B.; Stumpf, H. O.; Cano, J.; Lloret, F.; Julve, M. *Inorg. Chem*. **2013**, *15*, 8812−8819.

(12) Oliveira, W. X. C.; Ribeiro, M. A.; Pinheiro, C. B.; da Costa, M. M.; Fontes, A. P.; Nunes, W. C.; Cangussu, D.; Julve, M.; Stumpf, H. O.; Pereira, C. L. M. *Cryst. Growth Des.* **2015**, *3*, 1325−1335.

(13) Fernández, I.; Ruiz, R.; Faus, J.; Julve, M.; Lloret, F.; Cano, J.; Ottenwaelder, X.; Journaux, Y.; Munõz, M. C. *Angew. Chem. Int. Ed.* **2001**, *40*, 3039−3042.

(14) Ferrando-Soria, J.; Grancha, T.; Pasán, J.; Ruiz-Pérez, C.; Cañadillas-Delgado, L.; Journaux, Y.; Julve, M.; Cano, J.; Lloret, F.; Pardo, E. *Inorg. Chem.* **2012**, *13*, 7019−7021.

(15) Ruiz, R.; Faus, J.; Lloret, F.; Julve, M.; Journaux, Y. *Coord. Chem. Rev.* **1999**, *193−195*, 1069−1117.

(16) do Pim, W. D.; Oliveira, W. X. C.; Ribeiro, M. A.; de Faria, E. N.; Teixeira, I. F.; Stumpf, H. O.; Lago, R. M.; Pereira, C. L. M.; Pinheiro, C. B.; Figueiredo-Junior, J. C. D.; Nunes, W. C.; de Souza, P. P.; Pedroso, E. F.; Castellano, M.; Cano, J.; Julve, M. *Chem. Commun.* **2013**, *49*, 10778−10780.

(17) Simoes, T. R. G.; Mambrini, R. V.; Reis, D. O.; Marinho, M. V.; Ribeiro, M. A.; Pinheiro, C. B.; Ferrando-Soria, J.; Deniz, M.; Ruiz-Perez, C.; Cangussu, D.; Stumpf, H. O.; Lloret, F.; Julve, M. *Dalton Trans.* **2013**, *42*, 5778−579.

(18) Simoes, T. R. G.; do Pim, W. D.; Silva, I. F.; Oliveira, W. X. C.; Pinheiro, C. B.; Pereira, C. L. M.; Lloret, F.; Julve, M.; Stumpf, H. O. *CrystEngComm* **2013**, *15*, 10165−10170.

(19) Kahn, O. *Molecular Magnetism*, Wiley-VCH, Weinheim, 1993.

(20) Dul, M.-C.; Pardo, E.; Lescouëzec, R.; Journaux, Y.; Ferrando-Soria, J.; Ruiz-García, R.; Cano, J.; Julve, M.; Lloret, F.; Cangussu, D.; Pereira, C. L. M.; Stumpf, H. O.; Pasán, J.; Ruiz-Pérez, C. *Coord. Chem. Rev.* **2010**, *254*, 2281−2296

(21) Nowicka, B.; Korzeniak, T.; Stefańczyk, O.; Pinkowicz D.; Chorąży, S.; Podgajny, R.; Sieklucka, B. *Coord. Chem. Rev*. **2012**, *256*, 1946−1971.

(22) Janiak, C. *Dalton Trans.* **2003**, 2781−2804.

(23) Mroziński, J. *Coord. Chem. Rev*. **2005**, *249*, 2534−2548.

(24) Pardo, E.; Faus, J.; Julve, M.; Lloret, F.; Muñoz, M. C.; Cano, J.; Ottenwaelder, X.; Journaux, Y.; Carrasco, R.; Blay, G.; Fernández, I.; Ruiz-García, R.; *J. Am. Chem. Soc.* **2003**, *125*, 10770−10771.

(25) Castro, I.; Faus, J.; Julve M.; Amigó, J. M.; Sletten, J.; Debaerdemaeker, T. *J. Chem. Soc., Dalton Trans.* **1990**, 891-897.

(26) *CrysalisPro* Rigaku Oxford Diffraction, *CrysAlisPro Software system*, Rigaku Corporation, Oxford, UK, 2015.

(27) Sheldrick, G. M. *Acta Crystallogr*. **2008**, *A64*, 112.

(28) Palatinusz, L.; Chapuis, G. *J. Appl. Crystallogr.* **2007**, *40*, 786.

(29) Sheldrick, G. M. *SHELXL-97, Program for Crystal Structure Refinement*, University of Göttingen, Germany, 1997.

(30) Johnson, C. K. *ORTEP, Crystallographic Computing*, **1971**, edited by F. R. Ahmed, pp 217-219, Copenhagen, Denmark.

(31) Spek, A.L. *Acta Crystallogr.* **2009**, *D65*, 148−155.

(32) van der Sluis, P.; Spek, A. L. *Acta Crystallogr.*. **1990**, *A46*, 194−201.

(33) Lin, T.-P.; Gabba, F. P. *Angew. Chem. Int. Ed.* **2013**, *52*, 3864−3868.

(34) Macrae, C. F.; Bruno; I. J.: Chisholm, J. A.; Edgington, P. R.; McCabe, P.; Pidcock, E.; Rodríguez-Monge, L.; Taylor, R.; van de Streek, J.; Wood, P. A. *J. Appl. Crystallogr*. **2008**, *41*, 466−470.

(35) Nakamoto, K. *Infrared and Raman Spectra of Inorganic and Coordination Compounds, Part B: Applications in Coordination,Organometallic and Bioinorganic Chemistry*, Wiley-VCH: New York, 2009, pp 9−12, 79−82.

(36) Caires, F. J.; Lima, L. S.; Carvalho, C. T.; Siqueira, A. B.; Treu-Filho, O.; Ionashiro, M.; *J. Therm. Anal. Calorim.* **2012**, *107*, 335−344.

(37) Oliveira, W. X. C.; Ribeiro, M. A.; Pinheiro, C. B.; Nunes, W. C.; Julve, M.; Journaux, Y.; Stumpf, H. O.; Pereira, C. L. M. *Eur. J. Inorg. Chem*. **2012**, *34*, 5685−5693.

(38) Oliveira, W. X. C.; da Costa, M. M.; Fontes, A. P. S.; Pinheiro, C. B.; de Paula, F. C. S.; Jaimes, E. H. L.; Pedroso, E. F.; de Souza, P. P.; Pereira-Maia, E. C.; Pereira C. L. M. *Polyhedron* **2014**, *76*, 16−21.

(39) Fortea-Pérez, F. R.; Schlegel, I.; Julve, M.; Armentano, D.; De Munno, G.; Stiriba, S.E. *J. Organomet. Chem.* **2013**, *743*, 102−108.

(40) Fortea-Pérez, F. R.; Marino, N.; Armentano, D.; De Munno, G.; Julve, M.; Stiriba, S. E. *CrystEngComm* **2014**, *16*, 6971−6988.

(41) Fortea-Pérez, F. R.; Armentano, D.; Julve, M.; De Munno, G.; Stiriba, S. E.. *J. Coord. Chem.* **2014**, *67*, 4003-4015.

(42) Fortea-Pérez, F. R.; Rothenpieler, B. L.; Marino, N.; Armentano, D.; De Munno, G.; Julve, M.; Stiriba, S. E. *Inorg. Chem. Front.* **2015**, *2*, 1029−1039.

(43) Fortea-Pérez, F. R.; Neve, F.; Armentano, D.; De Munno, G.; Stiriba, S. E.; Julve, M. *Inorg. Chim. Acta* **2016**, *443*, 267-273.

(44) Lerner, E. I.; Lippard, S. J. *J. Am. Chem. Soc.* **1976**, *98*, 5397−5398.

(45) Lerner, E. I.; Lippard, S. J. *Inorg. Chem.* **1977**, *16*, 1546−1551.

(46) Folgado, J. V.; Coronado, E.; Beltrán-Porter, D.; Burriel, R.; Fuertes, A.; Miratvilles, C. *J. Chem. Soc., Dalton Trans.* **1988**, 3041−3046.

(47) Castro, I.; Sletten, J.; Faus, J.; Julve, M.; Journaux, Y.; Lloret, F.; Alvarez, S. *Inorg. Chem.* **1992**, *31*, 1889-1894.

(48) Sletten, J.; Julve, M.; Lloret, F.; Castro, I.; Seitz, G.; Mann, K. *Inorg. Chim. Acta* **1996**, 250, 219-225.

(49) Calatayud, M. L.; Castro I.; Sletten, J.; Lloret, F.; Julve, M. *Inorg. Chim. Acta* **2000**, *300-302*, 846-854.

(50) Cangussu de Castro Gomes, D.; Toma, L: M.; Stumpf, H. O.; Adams, H.; Thomas, J. A.; Lloret, F.; Julve, M. *Polyhedron* **2008**, *27*, 559-573.

(51) Carlucci, L.; Ciani, G.; Maggini, S.; Proserpio, D. M.; Sessoli, R.; Totti, F. *Inorg. Chim. Acta* **2011**, *376*, 538−548.

(52) Xu, W.; Pan, W.-J.; Zheng, Y.-Q. *J. Coord. Chem.* **2013**, *66*, 4415−4429.

(53) Addison, A. W.; Rao, N.; Reedijk, J.; van Rijn, J.; Verschoor, G. C. *J. Chem. Soc., Dalton Trans.* **1984**, 1349−1356.

(54) Aakeröy, C. B.; Hughes, D. P.; Nieuwenhuyzen, M. *J. Am. Chem. Soc*. **1996**, *118*, 10134−10140.

(55) Belmonte, M. M.; Price, D. J. *Acta Crystallogr*. **2010**, *C66*, o147−o150.

(56) Braga, D.; Grepioni, F.; Orpen, A. G. *Crystal Engineering: From Molecules and Crystals to Materials*, Springer Netherlands: Amsterdam, 1999.

(57) Lisnard, L.; Chamoreau, L.-M. ; Li, Y.; Journaux, Y. *Cryst. Growth Des.* **2012**, *10*, 4955−4962.

(58) Muñoz, M. C.; Blay, G.; Fernández, I.; Pedro, J. R.; Carrasco, R.; Castellano, M.; Ruiz-García, R.; Cano, J. *CrystEngComm* **2010**, *12*, 2473–2484.

(59) Stumpf, H. O.; Pei, Y.; Ouahab, L.; le Berre, F.; Codjovi, E.; Kahn, O. *Inorg. Chem*. **1993**, *32*, 5687−5691.

(60) Chun, H.; Salinas, B. H.; Bernal, H. *Eur. J. Inorg. Chem*. **1999**, *4*, 723−728.

(61) Pardo, E.; Ruíz-García, R.; Lloret, F.; Julve, M.; Cano, J.; Pasan, J.; Ruíz-Pérez, C.; Filali, Y.; Chamoreau, L. M.; Journaux, Y. *Inorg. Chem.* **2007**, *46*, 4504−4514 .

(62) Bleaney, B.; Bowers, K. D. *Proc. Roy. Soc. A* **1952**, *254*, 451−465.

(63) Chiari, B.; Helms, J. H.; Piovesana, O.; Tarantelli, T.; Zanazzi, P. F. *Inorg. Chem*. **1986**, *25*, 2408−2424.

(64) Hämäläinen, R.; Ahlgren, M.; Turpeinen, U. *Acta Crystallogr*. **1982**, *B38*, 1577−1580.

(65) Chiari, B.; Helms, J. H.; Piovesana, O.; Tarantelli, T.; Zanazzi, P. F. *Inorg. Chem*. **1986**, *25*, 870−874.

(66) Hernández-Molina, M.; González-Platas, J.; Ruiz-Pérez, C.; Lloret; F.; Julve, M. *Inorg. Chim. Acta* **1999**, *284*, 258−265.

(67) Grove, H.; Sletten, J.; Julve, M.; Lloret, F. *J. Chem. Soc., Dalton Trans.* **2001**, 2487−2493.

(68) De Munno, G.; Lombardi, M. G.; Julve, M.; Lloret, F.; Faus, J. *Inorg. Chim. Acta* **1998**, *282,* 82−89.

(69) Carranza, J.; Sletten, J.; Lloret, F.; Julve, M. *J. Mol. Struct.* **2008**, *890*, 31−34.

(70) Adhikary, C.; Koner, S. *Coord. Chem. Rev*. **2010**, *254*, 2933−2958.

(71) Cervera, B.; Ruiz, R.; Lloret, F.; Julve, M.; Cano, J.; Faus, J.; Bois, C.; Mroziński, J. *Coord. Chem. Rev*. **1997**, 395−401.

(72) Unamuno, I.; Gutiérrez-Zorrilla, J. M.; Luque, A.; Román, P.; Lezama, L.; Calvo, R.; Rojo, T. *Inorg. Chem.* **1998**, *37*, 6452−6460.

(73) da Cunha, T. T.; Oliveira, W. X. C.; Pinheiro, C. B.; Pedroso, E. F.; Nunes, W. C.; Pereira, C. L. M. *Cryst. Growth Des*. **2016**, *16*, 900−907.

(74) Ferrando-Soria, J.; Castellano, M.; Ruiz-García, R.; Cano, J.; Julve, M.; Lloret, F.; Ruiz-Pérez, C.; Pasán, J.; Cañadillas-Delgado, L.; Armentano, D.; Journaux, Y.; Pardo, E. *Chem.-Eur. J.* **2013**, *19*, 12124-12137.

(75) Pardo, E.; Cangussu, D.; Lescouëzec, R.; Journaux, Y.; Pasán, J.; Delgado, F. S.; Ruiz-Pérez, C.; Ruiz-García, R.; Cano, J.; Julve, M.; Lloret, F. *Inorg. Chem.* **2009**, *48*, 4661-4673.

For Table of Contents Use Only

Crystal engineering applied to modulate the structure and magnetic properties of oxamate complexes containing the $[Cu(bpca)]^+$ cation

Willian X. C. Oliveira,[†] Carlos B. Pinheiro,[‡] Marinez M. da Costa,[§] Ana P. S. Fontes,[⊥] Wallace C. Nunes,[‖] Francesc Lloret,[⊗] Miguel Julve[⊗] and Cynthia L. M. Pereira[†]*

TOC and short synopsis

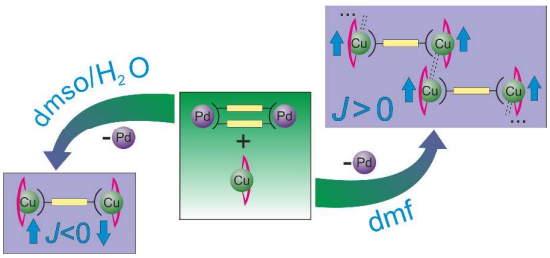

The *double-stranded* oxamato-based dipalladium(II) paracyclophane precursor undergoes an hydrolytic reaction in either dmf or dmso/water as solvents that in the presence of the bis(2-pyridylcarbonyl)amidatecopper(II) mononuclear complex leads to two new *single-stranded* oxamato-based copper(II) complexes with exhibit ferro- and antiferromagnetic interactions through the double oxo(carboxylate)-oxamate bridge and intermolecular contacts, respectively.